

WATER FILM FLOW IN A FRACTURE IN UNSATURATED POROUS MEDIUM

Prepared for

**Nuclear Regulatory Commission
Contract NRC-02-93-005**

Prepared by

**Center for Nuclear Waste Regulatory Analyses
San Antonio, Texas**

May 1994



**WATER FILM FLOW IN A FRACTURE
IN UNSATURATED POROUS MEDIUM**

Prepared for

**Nuclear Regulatory Commission
Contract NRC-02-93-005**

Prepared by

Vivek Kapoor

**Center for Nuclear Waste Regulatory Analyses
San Antonio, Texas**

May 1994

ABSTRACT

The evolution of a thin layer of water on an unsaturated porous incline is analyzed. A similarity solution is found for such flows incorporating the effects of gravity, viscosity, and an idealized linear representation of imbibition into the unsaturated porous matrix. The previously derived similarity solution for flow on an impervious surface by Huppert (1982) is a specific case of the new similarity solution. The maximum distance (the penetration length) that water can travel outside the porous medium is analytically related to the amount of water applied, acceleration due to gravity, the density and viscosity of water, the angle of inclination, and the rate of imbibition into the matrix. Using Green-Ampt and Richards' equation-based descriptions of the imbibition process, the evolution of water is numerically simulated. The penetration length and its variation with the amount of water applied to an unsaturated porous block are experimentally observed. By experimentally determining the imbibition rate, model predictions of the penetration length are compared to observations. The role of the distinct time scales of movement of water along the length of fractures and imbibition into the unsaturated porous matrix in determining the capacity of fractures to transport water in unsaturated porous media is discussed.

CONTENTS

Section	Page
FIGURES	v
TABLES	vi
SYMBOLS	vii
ACKNOWLEDGMENTS	viii
1 BACKGROUND	1-1
1.1 REGULATORY NEED	1-1
1.2 INDICATIONS OF FRACTURE FLOW AT YUCCA MOUNTAIN	1-2
1.3 MODELS OF FLOW IN VARIABLY SATURATED FRACTURED POROUS MEDIA	1-3
1.3.1 Heterogeneous Porous Continuum Approach	1-4
1.3.1.1 Discrete Fracture Models	1-4
1.3.1.2 Equivalent Continuum Models	1-4
1.3.2 Dual Continuum Approach	1-6
1.4 TECHNICAL OBJECTIVES	1-6
2 INTRODUCTION	2-1
2.1 ORGANIZATION	2-1
2.2 RELATIONSHIP WITH OTHER WORK	2-1
2.3 FORMULATION	2-2
2.3.1 Basic Equations	2-2
2.3.2 Thin-film Approximation	2-4
3 THIN-FILM FLOW WITH SIMPLIFIED IMBIBITION FUNCTIONS	3-1
3.1 SIMILARITY SOLUTION WITH FIRST ORDER LOSS TO POROUS MEDIUM	3-1
3.1.1 Penetration Length	3-4
3.1.2 Steady-State Solution for Dirichlet Upstream Boundary Condition	3-6
3.2 NUMERICAL APPROXIMATION FOR THIN-FILM FLOW	3-6
3.2.1 Zero Imbibition	3-9
3.2.2 First Order Imbibition	3-9
3.2.3 Green-Ampt Imbibition	3-9
4 THIN-FILM FLOW WITH RICHARDS' EQUATION-BASED IMBIBITION	4-1
4.1 NUMERICAL APPROXIMATION FOR VARIABLY SATURATED FLOW	4-1
4.2 COUPLED THIN-FILM VARIABLY SATURATED FLOW SIMULATION	4-5

CONTENTS (Cont'd)

Section		Page
5	EXPERIMENT	5-1
5.1	SETUP	5-1
5.2	ESTIMATION OF IMBIBITION COEFFICIENT	5-1
5.3	PREDICTIONS AND OBSERVATIONS OF PENETRATION LENGTH	5-2
6	DISCUSSION	6-1
6.1	FRACTURE EFFICACY NUMBER	6-3
7	SUMMARY AND RECOMMENDATIONS	7-1
8	REFERENCES	8-1

FIGURES

Figure		Page
2-1	Flow of a thin-film of water on an unsaturated porous incline	2-2
2-2	Film velocity	2-7
3-1	New similarity solution for thin-film flow with first order imbibition	3-3
3-2	Penetration length of water with first order imbibition	3-5
3-3	Position of leading edge of water film: comparison of first order imbibition and zero imbibition	3-7
3-4	Penetration length of water under Dirichlet upstream boundary condition, with first order imbibition	3-8
3-5a	Numerical approximation for thin-film flow: comparison with similarity solution for zero imbibition	3-10
3-5b	Numerical approximation for thin-film flow: comparison with new similarity solution for first order imbibition	3-11
3-6a	Numerical approximation of thin-film flow with Green-Ampt imbibition: evolution of water film and wetting front inside the porous medium	3-14
3-6b	Numerical approximation of thin-film flow with Green-Ampt imbibition: end points of water film	3-15
3-6c	Numerical approximation of thin-film flow with Green-Ampt imbibition: effect of varying initial height of water film	3-16
3-6d	Numerical approximation of thin-film flow with Green-Ampt imbibition: effect of changing angle of inclination	3-17
3-6e	Numerical approximation of thin-film flow with Green-Ampt imbibition: effect of changing Green-Ampt imbibition coefficient	3-18
4-1a	Evaluation of a modified MacCormack (1969) scheme for unsaturated flow: comparison with transient analytical solution to Burgers' equation	4-7
4-1b	Evaluation of a modified MacCormack (1969) scheme for unsaturated flow: comparison with steady-state analytical solution—Dirichlet boundary conditions	4-7
4-1c	Evaluation of a modified MacCormack (1969) scheme for unsaturated flow: comparison with steady-state analytical solution—Dirichlet and specified flux boundary condition	4-8
4-1d	Evaluation of a modified MacCormack (1969) scheme for unsaturated flow: convergence for transient moisture redistribution problem	4-8
4-2a	Numerical approximation of coupled thin-film—Darcy imbibition: evolution of water film and wetted zone inside the porous medium	4-9
4-2b	Numerical approximation of coupled thin-film—Darcy imbibition: end points of water film	4-10
5-1	Penetration length as a function of volume of water applied—experimental observations and model predictions	5-3

TABLES

Table	Page
5-1	Experimentally observed penetration lengths 5-2

SYMBOLS

FLUID CHARACTERISTICS:	ρ : Density of water, 1,000 kg/m ³ μ : Dynamic viscosity of water, 1.124×10^{-3} N s/m ² ν : Kinematic viscosity of water, 1.124×10^{-6} m ² /s
FIRST ORDER IMBIBITION PARAMETER:	κ : Imbibition coefficient, s ⁻¹
GREEN-AMPT IMBIBITION PARAMETERS:	K_{GA} : Hydraulic conductivity in Green-Ampt imbibition, m/s ψ_f : Suction head in front of wetted zone in Green-Ampt imbibition, m D_{GA} : Imbibition coefficient, m ² /s
GARDNER'S HYDRAULIC CONDUCTIVITY FUNCTION:	K_{sat} : Saturated hydraulic conductivity, m/s α_g : Gardner's alpha parameter, m ⁻¹
MOISTURE RETENTION FUNCTION:	$\theta(0)$: Volumetric moisture content at zero pressure head S_s : Specific storage coefficient, m ⁻¹ β : Moisture retention coefficient, m ⁻¹
OTHER:	p : Pressure (N/m ²) ψ : Suction head, $\psi \equiv -p/\rho g$ (m) k : Permeability (m ²) K : Hydraulic conductivity (m/s) θ_b : Initial volumetric moisture content θ_w : Wetted zone volumetric moisture content g : Acceleration due to gravity, 9.8 m/s ² α : Angle of porous incline, $0 < \alpha \leq \frac{\pi}{2}$ radians

ACKNOWLEDGMENTS

This report was prepared to document work performed by the Center for Nuclear Waste Regulatory Analyses (CNWRA) for the Nuclear Regulatory Commission (NRC) under Contract No. NRC-02-93-005. The activities reported here were performed on behalf of the NRC Office of Nuclear Regulatory Research, Division of Regulatory Applications. This report is an independent product of the CNWRA and does not necessarily reflect the views or regulatory position of the NRC.

The CNWRA-generated laboratory data contained in this report meets quality assurance (QA) requirements described in the CNWRA Quality Assurance Manual. For all other data, their respective sources should be consulted for determining their level of QA. The computer code developed to perform the analyses presented in this report is TFILM. This computer code is not presently controlled under the CNWRA Software Configuration Procedure TOP-018.

Gratefully acknowledged are discussions with R.G. Baca, S.A. Stothoff, A. Chowdhury, and G. Ofoegbu, and reviews by A.B. Gureghian, P.C. Lichtner, S. Mohanty, and W. Patrick.

1 BACKGROUND

1.1 REGULATORY NEED

An evaluation of the environmental consequences of the proposed high-level radioactive waste (HLW) repository at Yucca Mountain (YM) in southwest Nevada requires an assessment of the rates of water movement in the vadose zone. Since water is a potential carrier of radionuclides, larger time scales associated with its movement would support the feasibility of the geologic repository. The Nuclear Regulatory Commission (NRC), as a criterion for performance assessment (PA) of the proposed repository, has set a "Groundwater travel time criterion" that states:

"The geologic repository shall be located so that pre-waste emplacement groundwater travel time along the fastest path of likely radionuclide travel from the disturbed zone to the accessible environment shall be at least 1000 years or such other travel time as may be approved by the Commission." [Section 60.113(a)(2), 10 CFR Part 60 (Nuclear Regulatory Commission, 1991)]

Since the engineered containment for the radionuclides is expected to be effective for only a fraction of the half-lives of some of the radionuclides to be disposed, the geologic environment's ability to provide a barrier to the movement of radionuclides needs to be quantified to determine the feasibility of a geologic repository. The NRC stated, "The Commission considers both engineered and natural barriers to be important...." [Federal Register, page 28,203 (Nuclear Regulatory Commission, 1983)]. Therefore, the dissolution of radioactive waste in water and its subsequent movement in the natural environment needs to be anticipated. 10 CFR 60.112 specifically requires that:

"The release of radionuclides to the accessible environment must meet Environmental Protection Agency (EPA) standards."

The current EPA standards defined in 40 CFR Part 191 (Environmental Protection Agency, 1991) place a limit on the cumulative releases of radionuclides to the accessible environment for the first 10,000 yr after disposal (Section 191.13), and set a limit on the annual dose to any member of the public in the accessible environment during the first 1,000 yr after disposal (Section 191.15). The EPA in 40 CFR Part 191 also states that "disposal systems shall use different types of barriers to isolate the wastes from the accessible environment. Both engineered and natural barriers shall be included." (Section 191.14).

An assessment of the cumulative flux of solute across a specified boundary requires a description of the velocity field of the fluid transporting the solute from its source to the boundary. The radionuclides carried in the relatively rapid pathways would travel across a compliance boundary without undergoing as much radioactive decay as the radionuclides in the slower waters. The performance of the engineered containment for the radionuclides will also be influenced by its interaction with the water in the geologic environment. In this context, an evaluation of rates of water movement is needed to assess the suitability of the proposed site for HLW disposal.

1.2 INDICATIONS OF FRACTURE FLOW AT YUCCA MOUNTAIN

YM consists of a series of eastward dipping, variably welded fractured tuffaceous material. Some measurements reported in Scott et al. (1983), Montazer and Wilson (1984), and Peters et al. (1984, 1986) are presented here to describe the hydrostratigraphy of YM. Ababou (1991) provides a summary of this information in a review of modeling approaches. Wittmeyer et al. (1993) used rock-hydraulic property data, detailed microstratigraphic data, and measured saturation profiles in near-surface boreholes, to infer infiltration rates at YM. There is little alluvial cover above the proposed repository site, and the fractured welded Tiva Canyon unit crops out at the ground surface. Tiva Canyon is estimated to have 10 to 20 fractures per m^3 (Scott et al., 1983). The saturated matrix hydraulic conductivity of Tiva Canyon is of the order of 10^{-11} m/s, and matrix porosity is 10 percent. Beneath the Tiva Canyon unit lies the nonwelded Paintbrush Tuff unit, which is relatively less fractured (1 fracture per m^3) (Scott et al., 1983), and has a higher saturated matrix permeability (10^{-7} m/s) and porosity (40 percent) in comparison to the Tiva Canyon unit. The potential repository location is in the fractured welded Topopah Spring unit beneath the Paintbrush Tuff. Like Tiva Canyon, Topopah Spring is highly fractured with 8 to 40 fractures per m^3 (Scott et al., 1983). The saturated matrix permeability and porosity of Topopah Spring is of the same order as that of Tiva Canyon. The relatively less fractured Calico Hills nonwelded unit underlies Topopah Spring. The hydraulic properties of the consolidated porous matrix show variations within each unit, and the presence of fractures creates another strong variation in hydraulic properties superimposed on the matrix heterogeneity.

For an unfractured porous medium obeying the Darcy constitutive assumptions, measurements of *in situ* moisture contents or suction heads, along with the hydraulic conductivity-moisture content-suction head characteristics, provide an estimate of the flux of water. However, for a fractured porous medium the matrix moisture contents or suction heads may not provide an estimate of flux of water if the flux is predominantly due to transient fracture flow (Nitao et al., 1992). Most of the studies that infer infiltration rates at YM begin with the assumption that Richards' equation is sufficient for modeling flow of water in the fractured unsaturated porous medium. These studies either employ Darcy porous matrix constitutive properties, or "equivalent" continuum properties. These continuum properties are based on the presumption of pressure equilibrium between the fractures and the adjacent matrix. The analysis of infiltration into soils with macropores (Germann and Beven, 1981a,b; Beven and Germann, 1981, 1982) indicates that such an approach tends to underestimate infiltration by neglecting preferred pathways for downward water movement. In view of the limited and irregular alluvial cover and the cropping out of the fractured Tiva Canyon at the ground surface, the fact that "...the permeability of a soil during infiltration is mainly controlled by big pores, in which water is not held under the influence of capillary forces" (Schumacher, 1864) needs to be recognized in assessing infiltration at YM. The time scales associated with downward water movement in the porous matrix in the Tiva Canyon unit are large because the matrix saturated hydraulic conductivity divided by porosity is a small number (3.0 mm/yr). Based on this number, even if the Tiva Canyon unit were completely saturated, water would travel down only 3 m in 1,000 yr. It is likely that the time scale of evaporation processes is smaller than the time scale of downward water movement in the porous matrix; therefore little infiltration can be expected if water movement does indeed take place through the porous matrix. This scenario can change if the downward movement of water takes place in fractures, depending on the speed at which water moves in fractures and the amount of water imbibed by the porous matrix surrounding the fractures. A U.S. Department of Energy (DOE) peer-review team stated that there are "major uncertainties associated with" the process describing matrix-fracture interactions (Freeze, 1991). Considering that the dynamics of flow in unsaturated fractured porous medium are not well understood and that no large-scale controlled

infiltration experiments exist to directly determine the aggregate behavior of the fractured tuffaceous material at YM, the widely reported numerical model estimates of average annual infiltration rates are to be viewed with skepticism.

The average annual precipitation at YM is approximately 150 mm/yr. Rainfall, which is reported to be affected by surface topography, occurs as infrequent short intense thunderstorms that occasionally flood the nearby washes (Waddell et al., 1984). Nitao et al. (1992) have discussed evidence indicating that the nature of the precipitation and the hydraulic behavior of the fractured tuff render infiltration at YM to be spatially highly nonuniform. Some of the evidence they present indicating relatively rapid fracture flow at YM is repeated here.

- Detection of chlorine-36 and tritium at depths of 450 to 500 ft (Norris, 1989). At the rate of downward water movement characteristic to Tiva Canyon matrix properties (less than 3.0 mm/yr), thousands of years would be required for water to travel this distance.
- Loss of polymer-based drilling fluid while drilling borehole USW G-1 (Water Waste and Land Inc., 1986).
- Report by Quade and Cerling (1990) on stable isotope signatures for Trench 14, and comparison to pedogenic soil carbonates and spring deposits in the Amargosa Valley and Devils Hole. The Trench 14 data are similar to modern calcite deposited in soils from Piñon-Juniper vegetation zones. Similar measurements for calcite, filling fractures in cores taken from YM tuffs, were reported by Szabo and Kyser (1990). This similarity in the stable isotope ratios and the pedogenic origin of Trench 14 deposits indicate that the deposits in the fractures must be derived from percolating meteoric water (Nitao et al., 1992).

Yang (1992) analyzed tritium concentration profiles of test hole UE-25 UZ #4 in Pagany Wash near YM. He concluded that the tritium concentration inversions indicate "that non-vertical flow along preferential paths (fracture or channels) are occurring."

These empirical observations indicate that the potential for flow of water in fractures and faults is an important candidate for the fastest pathway for contaminant transport. The YM Site Characterization project has recognized this potential and the need to investigate it as part of site characterization activities (U.S. Department of Energy, 1988). On the modeling side, DOE-funded studies have also recognized this feature and have begun to model the dynamics of flow in discrete fractures interacting with variably saturated matrix to assess the environmental implications of the proposed HLW repository at YM (Travis et al., 1984; Nitao and Buscheck, 1991; Buscheck et al., 1991; Nitao et al., 1992; Zimmerman and Bodvarsson, 1992).

1.3 MODELS OF FLOW IN VARIABLY SATURATED FRACTURED POROUS MEDIA

Some current approaches for modeling flow in unsaturated fractured media are briefly reviewed here. For a more extensive discussion, the reader is referred to the review by Ababou (1991). Brown and Gelhar (1985) provide a critical review of flow in saturated fractured porous media. Manteufel et al. (1993) provide a detailed discussion of the coupling of thermal, mechanical, chemical, and hydrologic

processes. Ghosh et al. (1994) present an evaluation of computer codes for coupled thermal, mechanical, and hydrological process, pertinent to the proposed repository at YM.

1.3.1 Heterogeneous Porous Continuum Approach

In this approach, fractures are viewed as a porous medium with a contrasting hydraulic conductivity-moisture content-suction relationship. The presence of fractures completely filled with calcite supports their treatment as a distinct porous continuum, and a direct measurement of the properties of the fillings can provide the parameters needed to describe their flow behavior. For unfilled fractures, the hydraulic conductivity-saturation relationship can be constructed by assuming laminar flow (e.g., Beven and Germann, 1981). Wang and Narasimhan (1985) propose a suction-moisture content relationship for a fracture with a variable aperture, assuming capillary forces to be the dominant force on water inside a fracture. If the fracture surface and the dimensions of the water inside a fracture are such that capillary forces are not the dominant force on water in a fracture, water is subjected to an atmospheric pressure at its interface with air (assuming air to be infinitely mobile). If viscosity and gravity are important influences on water inside a fracture, it is possible for a fracture to go from complete saturation to small saturation values without the water pressure becoming negative. Therefore, it is not necessary to associate partial saturation of an unfilled fracture with negative fracture fluid pressure values. A large part of the range of hydraulic conductivities associated with a fracture can be in the positive pressure range. The aperture of the fracture and the nature of the fracture surface and its interaction with the fluid will determine the relative importance of viscosity, gravity, and capillary forces. The assignment of porous medium characteristics to unfilled fractures in unsaturated porous media needs to be experimentally investigated. Chuang et al. (1990) reported a fracture block experiment, but did not estimate a fracture hydraulic conductivity-pressure-moisture content relationship.

The heterogeneous porous continuum approach in modeling flow in unsaturated fractured porous media can be further divided into two categories: (i) discrete fracture models, and (ii) equivalent continuum models.

1.3.1.1 Discrete Fracture Models

If a geometric delineation of fractures based on observations or hypothesis is made, and they are assigned porous continuum properties, the resulting variably saturated flow problem can be presumably solved by a conventional unsaturated flow solver. If the hydraulic properties assigned to the fractures are appropriate, and the numerical approximation resolves the spatial-temporal variations of the suction field created due to fractures, this approach is an attractive one in understanding the behavior of fractured unsaturated porous medium. The work of Nitao and Buscheck (1991) is an example of an analytical approach to this problem. Baca et al. (1984) and Therrien (1992) have developed finite element techniques for simulating variably saturated flow with this approach. The difficulty with this approach is the assignment of Darcy constitutive properties to the fractures and computational requirements.

1.3.1.2 Equivalent Continuum Models

The starting point for assessing flow in this approach is similar to the discrete fracture approach, insofar as descriptions of the geometry and the constitutive properties of the fractures are required. The equivalent continuum approach seeks to replace the discrete fracture model of the porous medium with a simplified "equivalent" that is capable of predicting the spatially averaged flux of water in the discrete

fracture model. This approach is attractive because, after computing the constitutive parameters of the equivalent model, the task of predicting spatially averaged fluxes of fluid is rendered relatively simple. However, the development of a theoretical method to reduce a complex heterogeneous physical system into a simplified equivalent and testing its efficacy in predicting fluxes is a difficult task. *A priori*, the data requirements for this approach are not any less than the discrete fracture approach. However, if the equivalent constitutive properties of practical importance are shown to depend on certain statistical measures describing the fractures, such an approach has the potential for prioritizing data collection, and evaluating uncertainties due to limited data.

There is an important distinction to be made among methodologies to assign equivalent continuum properties to unsaturated heterogeneous porous medium. In one category, pressure equilibrium is assumed *a priori* in computing equivalent continuum parameters. The simplest of these approaches is to volumetrically average the assumed hydraulic conductivity-suction relationship, like Klavetter and Peters (1988). Also, the work of Mualem (1984) lies in this category. His work takes into account simple geometrical features of the heterogeneity orientation in numerically computing effective hydraulic conductivities, presuming pressure equilibrium. In the second category, there are analyses that explicitly calculate the suction head perturbations associated with flow in heterogeneous media and examine approximately how these perturbations, along with hydraulic conductivity perturbations, determine the capacity of the medium to transport water.

The theoretical results on steady-state unsaturated flow by Yeh et al. (1985) and Yeh (1989), on unsteady unsaturated flow by Mantoglou and Gelhar (1987), and the numerical work on steady-state unsaturated flow by Anderson and Shapiro (1983) are examples of approaches that examine the impact of suction head perturbations. This approach has been compared to experiments by Yeh and Harvey (1990). Polmann et al. (1988) and Gelhar (1993) provide a summary of the analytical results on assignment of effective properties incorporating the effects of suction head perturbations. Although the accomplishment of such a task analytically or numerically is based on simplifying approximations, the consideration of suction head perturbations in this approach has a major impact on the suction head dependant anisotropy and hysteresis of the computed effective hydraulic conductivity. This shows that the capacity of a heterogeneous soil to transmit water is greatly influenced by the suction head perturbations created due to material property variations. This approach has not been applied to the unsaturated fractured porous medium problem. If a realistic stochastic description of hydraulic properties of fractured porous medium can be made, the previously developed results for unfractured heterogeneous porous medium may be extended to fractured porous medium.

The work of Klavetter and Peters (1988) is attractive to the applied modeler because the effort involved in computing "effective" parameters is limited to adding two hydraulic conductivity-suction characteristics with different weights, reflecting the relative volumetric presence of fractures and porous matrix in a numerical grid block. The application of Klavetter and Peters method in modeling flow when the fractures are less conductive than the surrounding matrix is supported by Wang and Narasimhan (1985). However, it has been recognized that this approach will underestimate flux when fractured porous media are suddenly subjected to a wet boundary condition. This underestimation can be appreciated by a simple argument. If, during a rainfall event, water finds its way into fractures, it will flow relatively fast in the fracture due to a relatively large hydraulic conductivity. This rapid flow will occur until the water is imbibed into the adjacent matrix. However, in extensively fractured porous media, water may be able to travel considerable distances before it is imbibed into the matrix. In the Klavetter and Peters (1988) approach (presuming pressure equilibrium between fracture and adjacent matrix), this redistribution of moisture occurs instantaneously, thereby neglecting the distance water can travel before

this equilibration takes place. Once water is redistributed relatively uniformly, the fracture may become less conductive compared to the consolidated porous matrix. However, the fact that this approach unduly biases the velocities of water to the matrix values has been recognized in studies performed for the DOE (Nitao et al., 1992; Zimmerman and Bodvarsson, 1992). Rapid fracture flow is observed in a tunnel located 400 m beneath the top of Ranier Mesa (Russel et al., 1987), and the existence of dry porous matrix alongside a flowing fracture inside the tunnel is readily visible. If the fluid suction values along a horizontal transect through the fracture were to be measured, the fluid suction head would be relatively large away from the flowing fracture, and positive pressures could occur inside the fracture. To average the fluid suction value over the transect and assert that the flux of fluid can be computed by averaging the hydraulic conductivities evaluated at the average suction is the essence of the equivalent continuum approach which neglects the effect of suction variations in computing effective parameters. Since fractures are generally assigned hydraulic conductivities that decrease more rapidly with suction than the surrounding matrix, such a naive averaging approach would result in unduly large estimates of groundwater travel times at Ranier Mesa.

1.3.2 Dual Continuum Approach

In a dual continuum approach, the effect of fractures is sought to be represented as a distinct continuum with Darcy constitutive properties. The fracture continuum and the matrix continuum interact as they exchange fluids based on the pressure differences between them. This dual continuum approach is conceptually attractive because it permits water to travel at distinct rates in the distinct continua. It is less restrictive than the equivalent continuum models that make the critical fracture-matrix pressure equilibrium presumption (that makes them underestimate flux of water in fractured rocks subjected to wet boundary conditions.) However, the transfer function controlling the exchange of fluids in the dual continuum model needs to be theoretically determined, as the absence of any large-scale controlled experiment rules out its determination based on fitting to observations. A modeling exercise to determine the transfer term would have to employ a discrete fracture model and attempt to fit the right transfer term to make the dual continuum model yield the flux of water found in the discrete fracture model. *A priori*, the existence of a unique transfer term that will enable the dual continuum model to predict water flux in fractured unsaturated porous medium is not guaranteed. Updegraff et al. (1991) discuss the development of the dual continuum approach and its application to unsaturated fractured porous medium.

1.4 TECHNICAL OBJECTIVES

This study investigates fracture-matrix fluid flow interaction, incorporating viscous fluid motion physics and variably saturated porous medium behavior. A systematic development of theoretical concepts and experiments is needed to make a critical performance comparison of distinct modeling approaches, or develop an alternate approach to model flow in fractured unsaturated porous medium. Such a study would encompass experiments on laboratory-scale matrix blocks with and without fractures, large-block experiments, and controlled field-scale experimentation. However, the objective of this study is limited to developing an understanding of the phenomenon of a thin layer of water dripping down a fracture in an unsaturated porous medium. The focus in this work is on the disparate rates of water movement in consolidated porous medium and on water movement in unfilled fractures. The imbibition of water into the porous matrix, the manner in which it determines the proportion in which these velocities are experienced by water, and the distances and rates at which water travels are analytically and numerically studied. Observations from a simple experiment conducted in this study are compared to model predictions. The analysis made here assumes isothermal conditions.

2 INTRODUCTION

2.1 ORGANIZATION

The evolution of a thin layer of water on an idealized plane unsaturated porous medium (Figure 2-1) is examined in this work. Section 2.3 formulates the nonlinear initial-boundary value problem governing the spatial-temporal evolution of water dictated by the constitutive properties of the water and porous continuum, and by the conservation of fluid mass and momentum under isothermal conditions. A similarity solution for such flows is reported in Section 3.1, coupling the nonlinear advection equation governing the evolution of water outside the porous medium to an idealized linear representation of water loss to the porous medium. The derived similarity solution yields analytical expressions of the maximum distance a finite amount of water can travel outside the porous medium before becoming completely imbibed. This maximum distance is referred to as the "penetration length." Numerical approximations to model such flows are evaluated by comparison with similarity solutions in Section 3.2. The evolution of the thin layer of water with imbibition into porous medium modeled using the Green-Ampt model and Richards' equation, is numerically simulated in Sections 3.2 and 4, respectively. A simple experiment of this phenomenon is reported in Section 5, where observed penetration lengths are compared to model predictions employing the Green-Ampt imbibition model. A discussion and a summary of the results of this study are provided in Sections 6 and 7 respectively.

2.2 RELATIONSHIP WITH OTHER WORK

The juxtaposition of unsaturated flow and viscous flows to examine the interaction of viscous transport of fluid momentum, gravitational acceleration of the fluid, and the loss of fluid to the unsaturated porous medium is the objective of this work. The nonlinear equation used in this study to model the flow of water outside the porous medium is a specific case of the kinematic wave equation, which has been used previously to numerically study surface hydrological response and infiltration (e.g., Henderson and Wooding, 1964; Chen, 1970; Smith and Woolhiser, 1971; Li et al., 1975; Smith and Hebbert, 1979; Cundy and Tonto, 1985; Luce and Cundy, 1992). Beven and Germann (1981) numerically coupled steady-state viscous flow descriptions and unsaturated flow for vertical cylindrical pores in unsaturated porous medium. Davidson (1984) modeled the imbibition of water into unsaturated porous medium from a crack, employing a two-dimensional (2D) Green-Ampt model, neglecting gravity. The crack was assumed to be full of water under hydrostatic conditions in Davidson's work. In contrast to earlier works, the focus of this study is on the maximum travel distance (penetration length) for a specified amount of water introduced on low-permeability consolidated porous medium. In the fluid mechanics literature on flow on impervious surfaces, a viscous-gravity balance has been previously employed to describe the fluid flow via similarity solutions, and favorable comparison between theory and observation have been found (e.g., Smith, 1973; Huppert, 1982; Lister, 1992). The analytical, numerical, and experimental results developed here generalize this class of previous work insofar as the effects of the imbibition of water into the porous medium are incorporated.

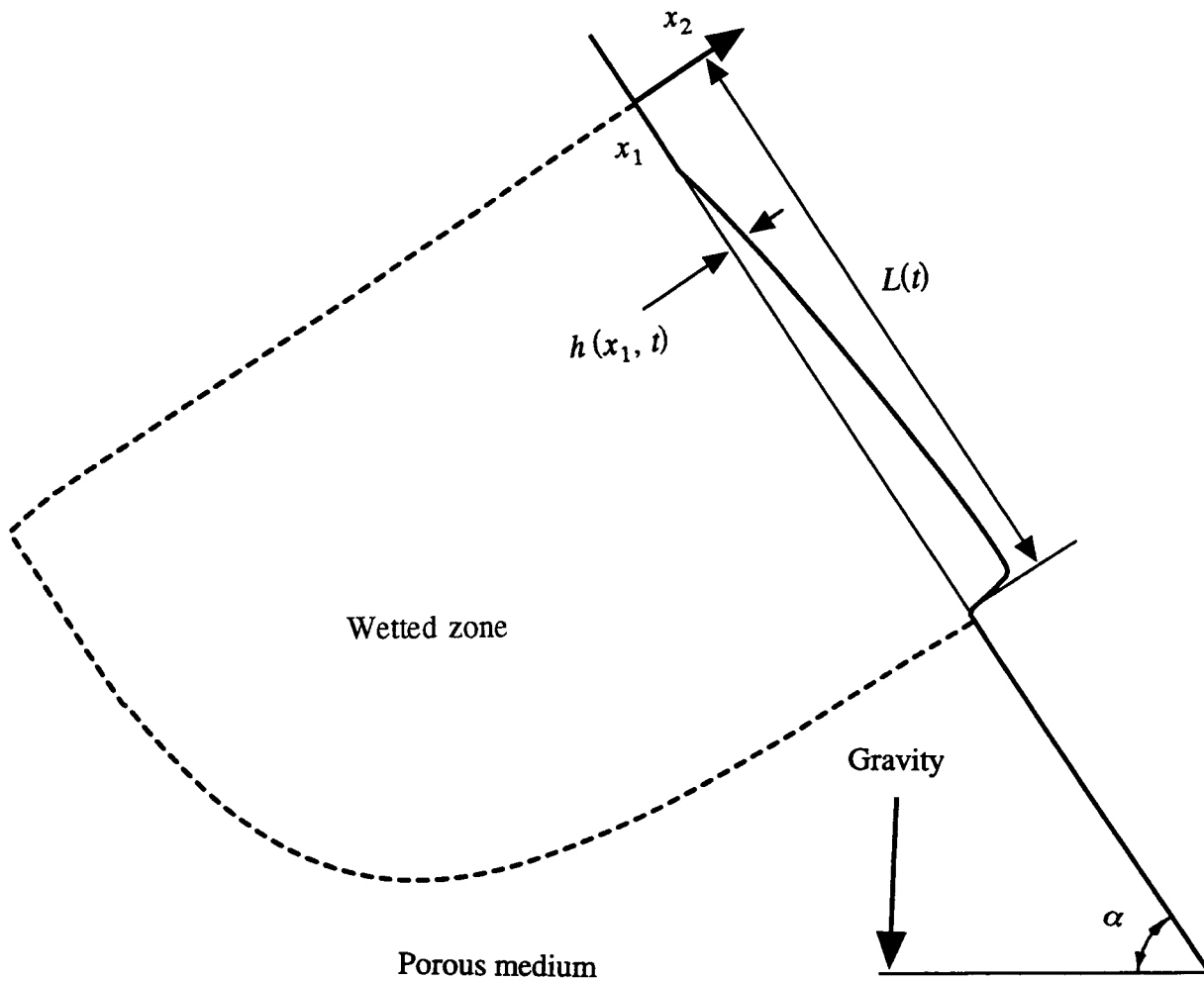


Figure 2-1. Flow of a thin film of water on an unsaturated porous incline

2.3 FORMULATION

2.3.1 Basic Equations

The conservation of an incompressible fluids momentum and mass dictate that

$$\rho \left(\frac{\partial u_i}{\partial t} + u_j \frac{\partial u_i}{\partial x_j} \right) = - \frac{\partial p}{\partial x_i} + \rho g_i + \mu \frac{\partial^2 u_i}{\partial x_j^2} \quad (2-1)$$

and

$$\frac{\partial u_i}{\partial x_i} = 0 \quad (2-2)$$

In Eq. (2-1), ρ is the density of water, p is the pressure, μ the dynamic viscosity of water, g_i is the component of the acceleration of gravity in the i th direction, and u_i is the velocity of water. A summation over repeated indices is implied in Eqs. (2-1) and (2-2). Inside the porous medium, the flux of water q_i is assumed to be governed by the Darcy porous continuum constitutive model

$$q_i = - \frac{k}{\mu} \left(\frac{\partial p}{\partial x_i} - \rho g_i \right) \quad (2-3)$$

For the coordinate system shown in Figure 2-1, $g_1 = g \sin(\alpha)$ and $g_2 = -g \cos(\alpha)$. Assuming ρ to be a constant, conservation of fluid mass inside the porous continuum is expressed as

$$\frac{\partial \theta}{\partial t} + \frac{\partial q_i}{\partial x_i} = 0 \quad (2-4a)$$

A sum over repeated indices is implied in Eq. (2-4a) in which θ is the volume of water per unit bulk porous medium volume. In Eq. (2-3), k is the permeability of the isotropic porous medium. Equations (2-3) and (2-4a), along with functions $k(p)$ and $\theta(p)$, determine the porous medium flow mechanisms. The microstructure of the porous medium and its interaction with fluid determine $k(p)$ and $\theta(p)$. Relating these functions to the pore-scale geometry is difficult in view of their dependence on complex 3D pore geometry and physical processes. A direct measurement of these porous medium constitutive functions is needed in practical applications. Equation (2-4a) implies that the soil-water suction head $\psi = -p/\rho g$ (assuming constant fluid density ρ) is governed by a form of Richards' equation (Richards', 1931)

$$\begin{aligned} S \frac{\partial \psi}{\partial t} + \frac{\partial}{\partial x_1} \left[-K(\psi) \sin(\alpha) - K(\psi) \frac{\partial \psi}{\partial x_1} \right] \\ + \frac{\partial}{\partial x_2} \left[K(\psi) \cos(\alpha) - K(\psi) \frac{\partial \psi}{\partial x_2} \right] = 0 \end{aligned} \quad (2-4b)$$

where

$$S = - \frac{d\theta}{d\psi} \quad (2-4c)$$

In Eq. (2-4b), hydraulic conductivity $K = k \rho g / \mu$, the x_1 axis is assumed to be dipping at an angle α below the horizontal direction, and the x_2 axis is at an angle α in the clockwise direction from the vertical (Figure 2-1.) For positive suction head values, the coefficient S represents the effects of change

in storage of moisture with suction. For positive pressure values and an incompressible fluid, S represents the effects of compressibility of the porous medium. For saturated conditions, S is typically of the order of 10^{-4} m^{-1} for unconsolidated material (Hunt, 1983). If the coefficient S were set to zero, Eq. (2-4b) would become an elliptic equation. In the variably saturated porous medium flow problem analyzed here, there is a possibility that some regions are completely saturated. In this circumstance, retaining a positive value for S at positive pressures (attributed to porous medium compressibility) provides a continuous variation of S between fully saturated and unsaturated flows. Depending on the function $\theta(\psi)$, there may be a strong disparity between the time constants over which the pressure field changes are propagated in these distinct porous flow regimes.

In addition to Eqs. (2-1) through (2-4a,b,c), the conditions at the interface between the water outside the porous medium and the water inside the porous medium need to be specified. The details of the hydrodynamics of water entering pore spaces are not modeled here. For the free surface water outside the porous medium, it is assumed that the velocity at the interface, tangential to the porous plane, is zero. The velocity component orthogonal to the interface is equal to the normal flux of water inside the porous matrix, which is also governed by the porous medium flow mechanisms. Additionally, the pressure at the interface is assumed to be uniquely defined. The appropriateness of these interface conditions between free flows and porous flows has been debated because of the distinct scales at which the continuum hypothesis is made in the distinct media. For example, the tangential velocity of fluid particles at the interface admits a discontinuity in this boundary condition specification. This discontinuity is because the porous flow problem does not involve second derivatives of the velocity, unlike Navier-Stokes equations. The reader is referred to analysis by Taylor (1971) and Saffman (1971), experiments by Beavers and Joseph (1967) and Beavers et al. (1970) and (1974), and the recent pore-scale numerical modeling work by Martys et al. (1994) for an investigation of boundary conditions between free flows and saturated porous media flows.

2.3.2 Thin-film Approximation

A free surface flow governed by the Navier-Stokes equations [Eq. (2-1)] is rendered simpler under the thin-film approximation

$$h \ll L, \quad h \frac{\partial h}{\partial t} \ll \nu \quad (2-5a)$$

where h is the thickness of the layer of water, L is the characteristic longitudinal length of the water body, and $\nu = \mu/\rho$ is the kinematic viscosity of water. Under these conditions, Eq. (2-1) is approximated in two dimensions as

$$0 = - \frac{1}{\rho} \frac{\partial p}{\partial x_1} + \nu \frac{\partial^2 u_1}{\partial x_2^2} + g \sin(\alpha) \quad (2-5b)$$

and

$$0 = -\frac{1}{\rho} \frac{\partial p}{\partial x_2} - g \cos(\alpha) \quad (2-5c)$$

The reduction of the Navier-Stokes equations [Eq. (2-1)] to the thin-film equations [Eqs. (2-5b,c)] is discussed in fluid mechanics texts (Acheson, 1989). Conditions specified in Eq. (2-5a) ensure that the spatial derivatives of the velocity in the x_1 direction are much smaller than those in the x_2 direction, and that the terms on the left side of Eq. (2-1) are small. For the thin-film approximations to apply, it is not necessary for the Reynolds number (based on the longitudinal length scale L) to be small, provided that h/L is sufficiently small. The pressure in the fluid is obtained by solving Eq. (2-5c)

$$p = \rho g(h - x_2) \cos(\alpha) + p_A \quad (2-6)$$

where p_A is the atmospheric pressure. Henceforth, p_A is set to zero, therefore, fluid pressure values are expressed relative to atmospheric pressure. Substituting Eq. (2-6) in Eq. (2-5b) yields

$$v \frac{\partial^2 u_1}{\partial x_2^2} = -g \sin(\alpha) + g \frac{\partial h}{\partial x_1} \cos(\alpha) \quad (2-7)$$

Consistent with the thin-film approximation [Eq. (2-5a)], the second term on the right side of Eq. (2-7) may be considered to be small compared to the first term, for nonzero or very small values of α , and is neglected. The zero tangential stress condition and the purely kinematic condition at the top of the layer of water require that

$$\mu \frac{\partial u_1}{\partial x_2} = 0, u_2 = \frac{\partial h}{\partial t} + u_1 \frac{\partial h}{\partial x_1}; x_2 = h \quad (2-8)$$

Equations (2-7) and (2-8) and the incompressibility condition [Eq. (2-2)] yield the equation governing the evolution of the thickness h of the thin-film of water outside the porous medium

$$\frac{\partial h}{\partial t} + ch^2 \frac{\partial h}{\partial x_1} = s, s(x_1, t) = u_2(x_1, x_2 = 0, t) \quad (2-9a)$$

$$c = \frac{\rho g \sin(\alpha)}{\mu}$$

The divergence-free 2D fluid velocity in the thin-film of water is obtained from Eqs. (2-7), (2-8), and the incompressibility condition of Eq. (2-2)

$$u_1(x_1, x_2, t) = \frac{\rho g \sin(\alpha)}{\mu} \left[h(x_1, t)x_2 - \frac{x_2^2}{2} \right] \quad (2-9b)$$

$$u_2(x_1, x_2, t) = u_2(x_1, x_2 = 0, t) - \frac{x_2^2}{2} \frac{\rho g \sin(\alpha)}{\mu} \frac{\partial h(x_1, t)}{\partial x_1}$$

This velocity description may be used to model solute transport. In this work, the focus is on Eq. (2-9a), which enables a direct study of the evolution of the thickness of the water film without solving for the details of its velocity field. This affords a 2D analysis of the water flowing on the porous medium.

In Eq. (2-9a), the fluid velocity s at the interface, orthogonal to the porous plane, provides a coupling between the water outside the porous medium with the flux inside it. Negative values of s signifying water loss to the porous medium create a reduction in film thickness h , which causes a reduction in its velocity ch^2 , which reflects a balance between viscous effects and gravity. An appreciation of the impact of gravity and viscosity on layers of water of different thickness can be obtained from Figure 2-2, which shows how the film velocity ch^2 varies with its thickness and the angle of inclination. Gravity has the potential to make even very thin layers of water travel relatively fast outside the porous medium. However as a finite size water body introduced onto a porous incline moves, its thickness decreases, and thereby its velocity is reduced. The description of how this happens on an idealized plane unsaturated porous surface and an assessment of the impact of water loss to the porous medium on the movement of water are presented in the following sections.

2-7

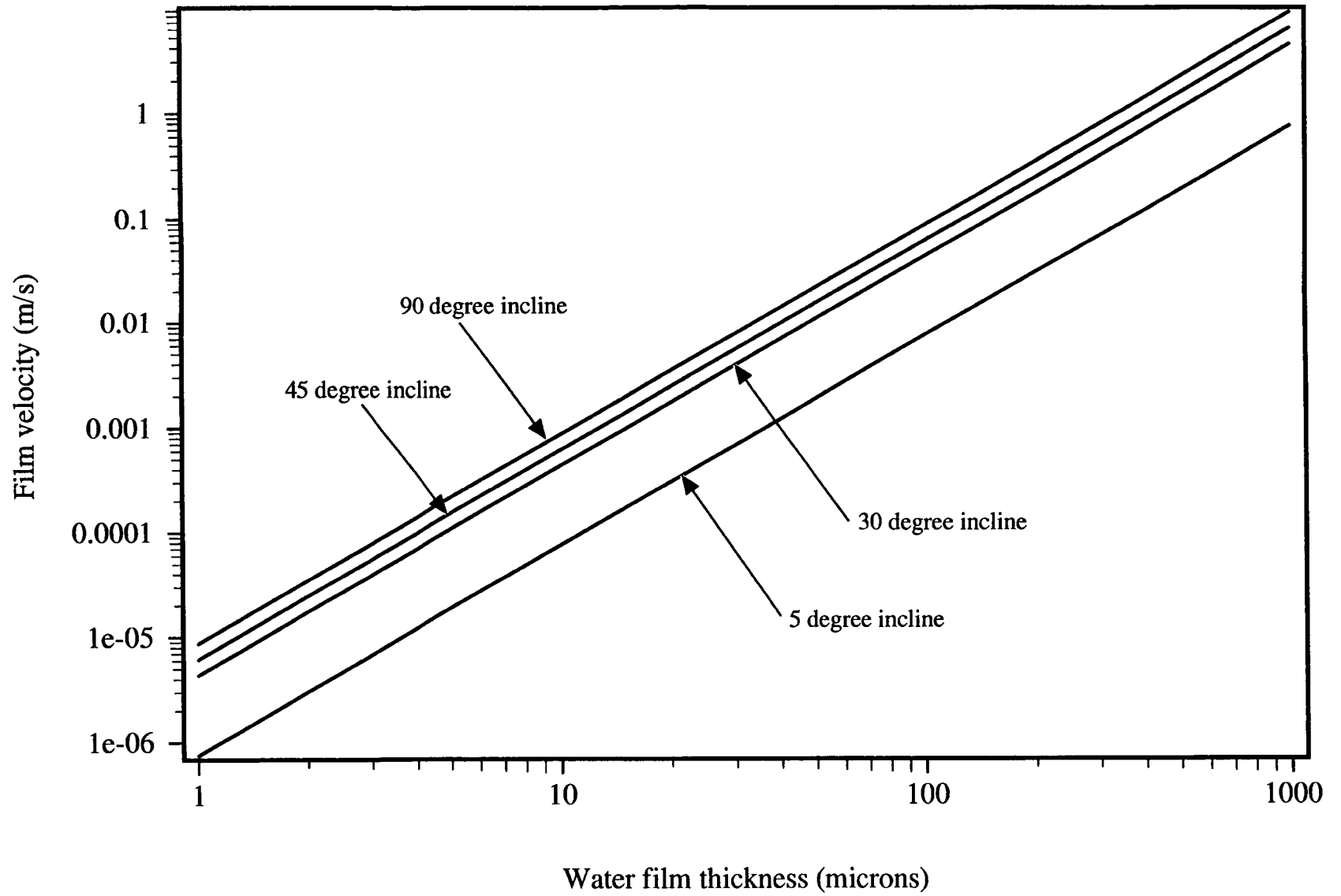


Figure 2-2. Film velocity

3 THIN-FILM FLOW WITH SIMPLIFIED IMBIBITION FUNCTIONS

The evolution of a viscous fluid on impervious surfaces has been extensively studied employing the thin-film approximation [Eq. (2-9a)]. Solutions to these thin-film equations have been found without any water loss term (e.g., Smith, 1973, Huppert, 1982, Lister, 1992). For a linear model of imbibition of water into the porous medium, a new similarity solution to Eq. (2-9a) is developed here. This solution affords an exploration of the parametric sensitivities of this fluid flow-imbibition phenomenon, and also provides a method to evaluate the numerical approximations for the thin-film equation with a loss term. The numerical approximation is then used to examine the influence of different representations of the imbibition process.

3.1 SIMILARITY SOLUTION WITH FIRST ORDER LOSS TO POROUS MEDIUM

To begin examining the properties of solutions to Eq. (2-9a), consider the loss of water to the porous medium at a rate proportional to the pressure at the interface, that is, $s = -\kappa h$. This is a very simplified representation of the imbibition process into unsaturated porous medium. If the time scale of loss of water is small compared to the time scale associated with the movement of water outside the porous medium, that is, if κ is much greater than $cA^2/L^3(0)$, with A being the initial area of water body on the porous medium and $L(0)$ its initial longitudinal dimension, water barely moves down the porous incline before it is lost to the porous medium due to imbibition. In this circumstance, the solution to the evolution of water is simply an exponential decrease of the height of water outside the porous medium. However, if the imbibition rate constant κ is less than $cA^2/L^3(0)$, then the thin layer of water can be expected to move down the incline.

In order to solve Eq. (2-9a) with $s = -\kappa h$, first consider the general nonlinear-temporally varying advection equation

$$\frac{\partial h}{\partial t} + g(t) N(h) \frac{\partial h}{\partial x} = 0 \quad (3-1)$$

Where $N(h)$ is a nonlinear function of h . Equation (3-1) admits general solutions of the form

$$f \left[x - N(h) \int_0^t g(\tau) d\tau \right] \quad (3-2)$$

for an arbitrary function f . Under the condition that N^{-1} is a single-valued function, Eq. (3-2) yields similarity solutions for h of the form

$$h = N^{-1} \left[\frac{x}{\int_0^t g(\tau) d\tau} \right] \quad (3-3)$$

Differentiation of Eqs. (3-2) and (3-3) shows that they satisfy Eq. (3-1). For a first order loss function ($s = -\kappa h$), Eq. (2-9a) can be readily transformed into the form of Eq. (3-1) [by making the transformation $h^* = h \exp(\kappa t)$] for an impulsive introduction of water on the porous surface. From Eq. (3-3), the similarity solution to Eq. (2-9a) with a linear loss function may be constructed

$$h(x_1, t) = \sqrt{\frac{2\kappa\mu x_1 e^{-2\kappa t}}{\rho g \sin(\alpha)(1 - e^{-2\kappa t})}} \quad (3-4)$$

The solution in Eq. (3-4) can be expected to govern the main part of the water body outside the porous medium, independent of the initial conditions, after the water body has traveled down distances of the order of its original longitudinal dimensions, which happens when t is greater than $L^3(0)/cA^2$. A differentiation of the solution [Eq. (3-4)] shows that it satisfies Eq. (2-9a) with a first order loss function. The position of the advancing tip of the thin layer of water may be found by integrating Eq. (3-4) and recognizing that the total area of water outside the porous medium will be decaying exponentially. These evaluations yield the position of the leading edge of the water body

$$L(t) = \left[\frac{9}{8} \frac{A^2 \rho g \sin(\alpha)}{\kappa\mu} (1 - e^{-2\kappa t}) \right]^{1/3} \quad (3-5)$$

Equivalently, the time at which point $x_1 > 0$ is hit by the leading edge of water is given by expression

$$t_h(x_1) = -\frac{1}{2\kappa} \ln \left[1 - \frac{8x_1^3 \kappa\mu}{9A^2 \rho g \sin(\alpha)} \right] \quad (3-6)$$

Of course, Eq. (3-6) is valid only for positive arguments of the logarithm. Figure 3-1 presents a schematic of the new similarity solution [Eqs. (3-4) through (3-6)].

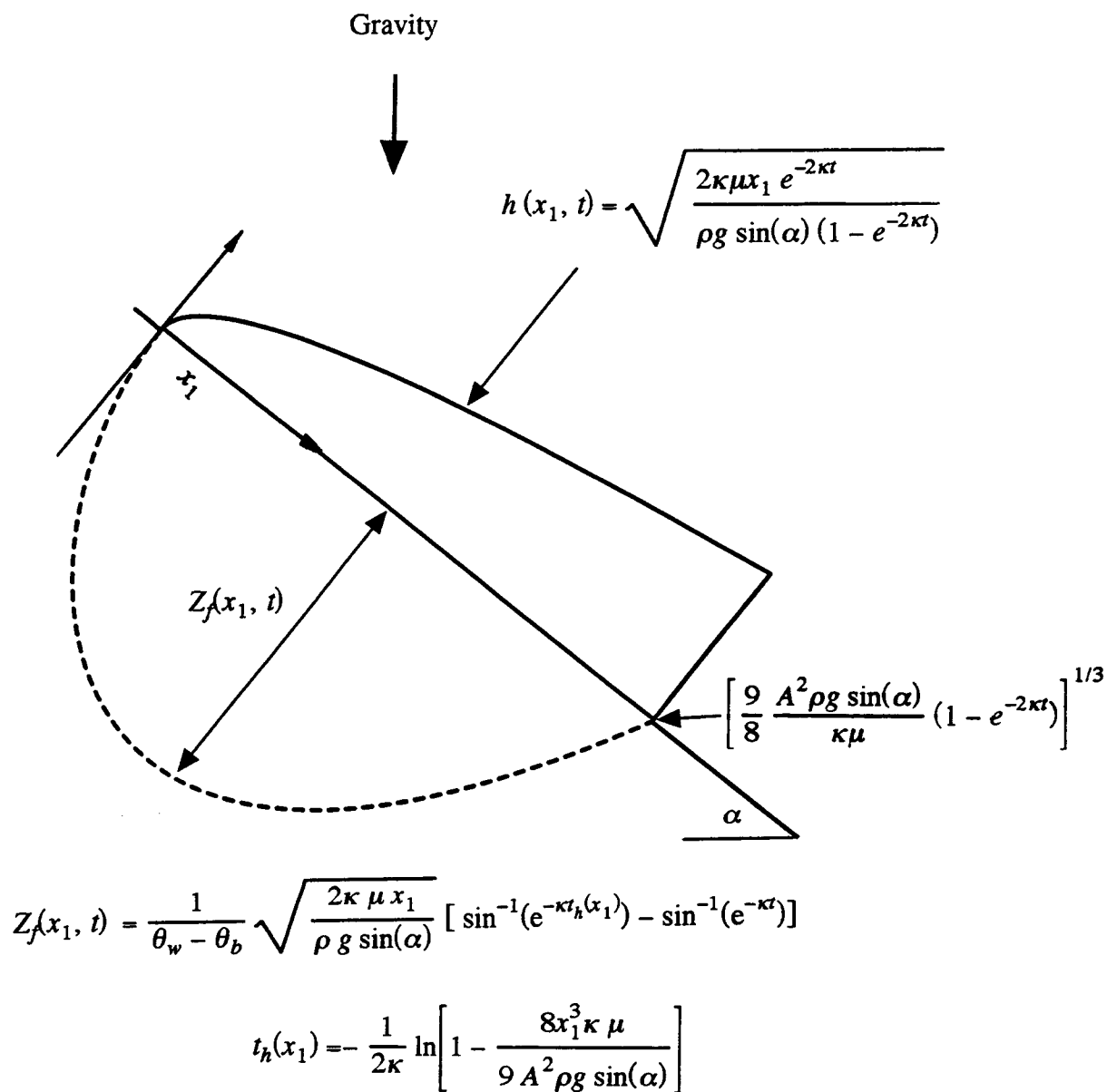


Figure 3-1. New similarity solution for thin-film flow with first order imbibition

3.1.1 Penetration Length

It follows from Eq. (3-5) that

$$\lim_{t \rightarrow \infty} L(t) \rightarrow \left[\frac{9}{8} \frac{A^2 \rho g \sin(\alpha)}{\kappa \mu} \right]^{1/3} \quad (3-7)$$

Therefore, the thin-film Eq. (2-9a) with a first order loss yields distinct penetration lengths beyond which the thin layer of water cannot travel. Equation (3-7) shows the sensitivities of this distinct length to the physical variables controlling the flow problem. Figure 3-2 presents the variation of the penetration length with the initial height of the film of water. The similarity solution is expected to hold if the water body has traveled a distance comparable to its original length, $L(0)$. This condition occurs if the initial thickness of the water film is larger than the amount indicated beneath the vertical line in Figure 3-2. Of course, the first order imbibition is a major simplification of the dynamics of imbibition by the porous medium. However, the qualitative behavior of the nonlinear-advection-source/sink term Eq. (2-9a) is revealed by the derived similarity solution [Eqs. (3-5) to (3-7)]. Employing the first order loss model for imbibition of water into the porous medium as a sharp front, the depth of the wetting front inside the porous medium $Z_f(x_1, t)$ is governed by

$$(\theta_w - \theta_b) \frac{dZ_f(x_1, t)}{dt} = \kappa h(x_1, t) \quad (3-8a)$$

which is equivalent to

$$Z_f(x_1, t) = \frac{\kappa}{\theta_w - \theta_b} \int_{t_h(x_1)}^t h(x_1, \tau) d\tau \quad (3-8b)$$

θ_b and θ_w are the initial moisture content and wetted zone moisture content, respectively. Equations (3-4), (3-6), and (3-8) yield a simple expression for the position of the advancing wetting front inside the porous medium

$$Z_f(x_1, t) = \frac{1}{\theta_w - \theta_b} \sqrt{\frac{2\kappa\mu x_1}{\rho g \sin(\alpha)}} \left\{ \sin^{-1} [e^{-\kappa t_h(x_1)}] - \sin^{-1}(e^{-\kappa t}) \right\} \quad (3-9)$$

A schematic of this solution is shown in Figure 3-1.

The similarity solutions constructed above yield the similarity solution for flow down an impervious slope when the amount of water imbibed by the porous medium is small, that is, when $\kappa t \ll 1$, Eqs. (3-4) and (3-5) become

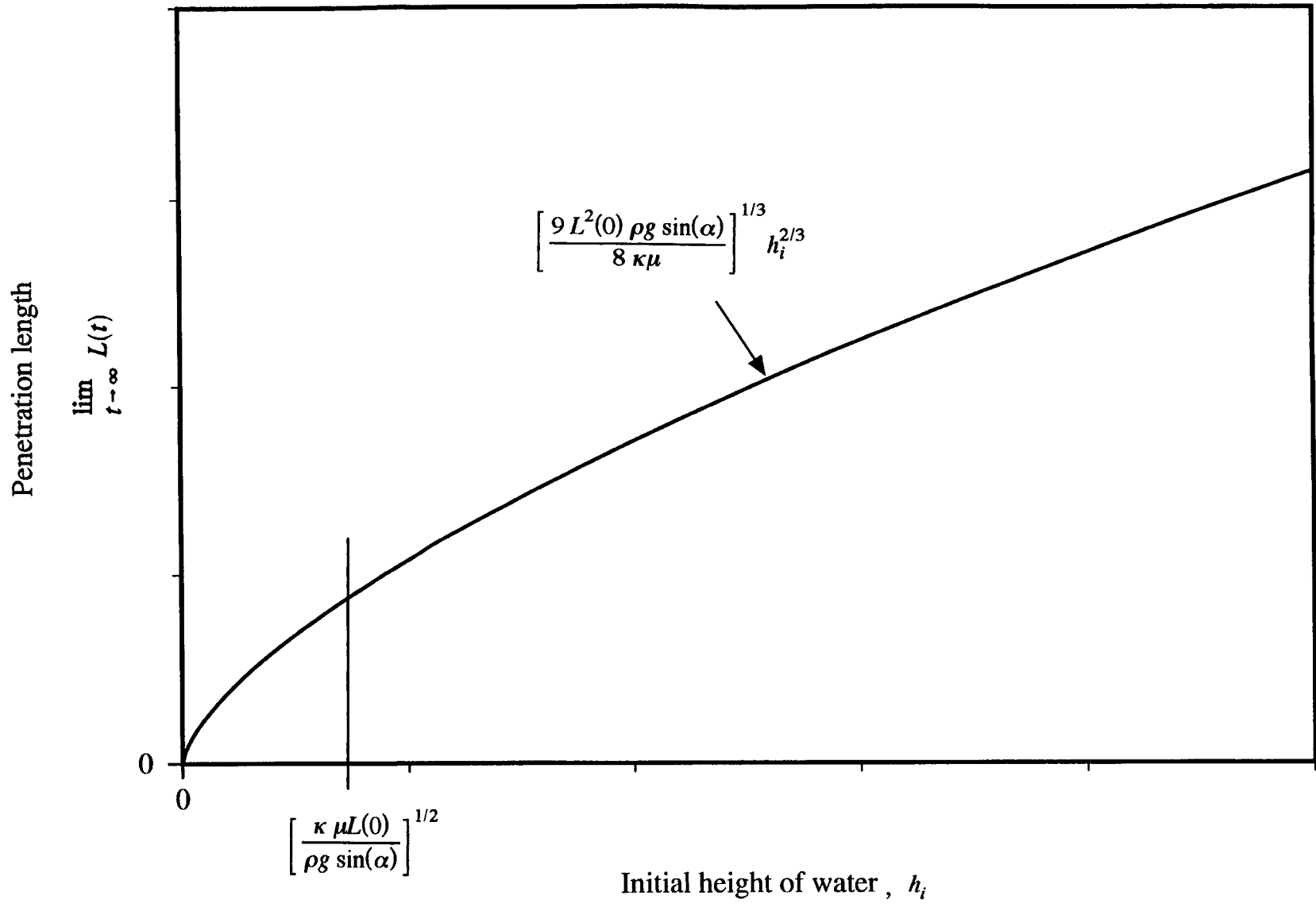


Figure 3-2. Penetration length of water with first order imbibition

$$h(x_1, t) = \sqrt{\frac{x_1 \mu}{t \rho g \sin(\alpha)}} \quad (3-10)$$

and

$$L(t) = \left[\frac{9A^2 \rho g \sin(\alpha) t}{4 \mu} \right]^{1/3} \quad (3-11)$$

Expressions (3-10) and (3-11) were presented by Huppert (1982). The contrasting nature of the temporal evolution of the water body with no imbibition and with a first order imbibition function is shown in Figure 3-3.

3.1.2 Steady-State Solution for Dirichlet Upstream Boundary Condition

The previous derivations pertain to the evolution of a finite amount of water impulsively introduced onto the porous medium. Also of interest is the case in which a specified height of water is maintained at the upstream end of a porous plane. Specifying the height of water fixes the flux of water. Figure 3-4 illustrates the situation in which an idealized parallel plate fracture at an inclination is subjected to incipient ponding. For a first order loss function, the steady-state solution to Eq. (2-9a) yields a finite penetration length

$$\lim_{t \rightarrow \infty} L(t) = \frac{\rho g \sin(\alpha) h_i^2}{2 \kappa \mu} \quad (3-12)$$

Equation (3-12) was obtained by setting the temporal derivative in Eq. (2-9a) to zero, and solving the resultant ordinary differential equation for h^2 . The penetration length Eq. (3-12) reflects a balance in which the rate at which water is being applied is equal to the rate at which water is being imbibed into the porous medium.

3.2 NUMERICAL APPROXIMATION FOR THIN-FILM FLOW

To further explore the coupled flow of water on and in an unsaturated porous medium, numerical approximations of the thin-film Eq. (2-9a) are developed here. The three-step explicit scheme employed is

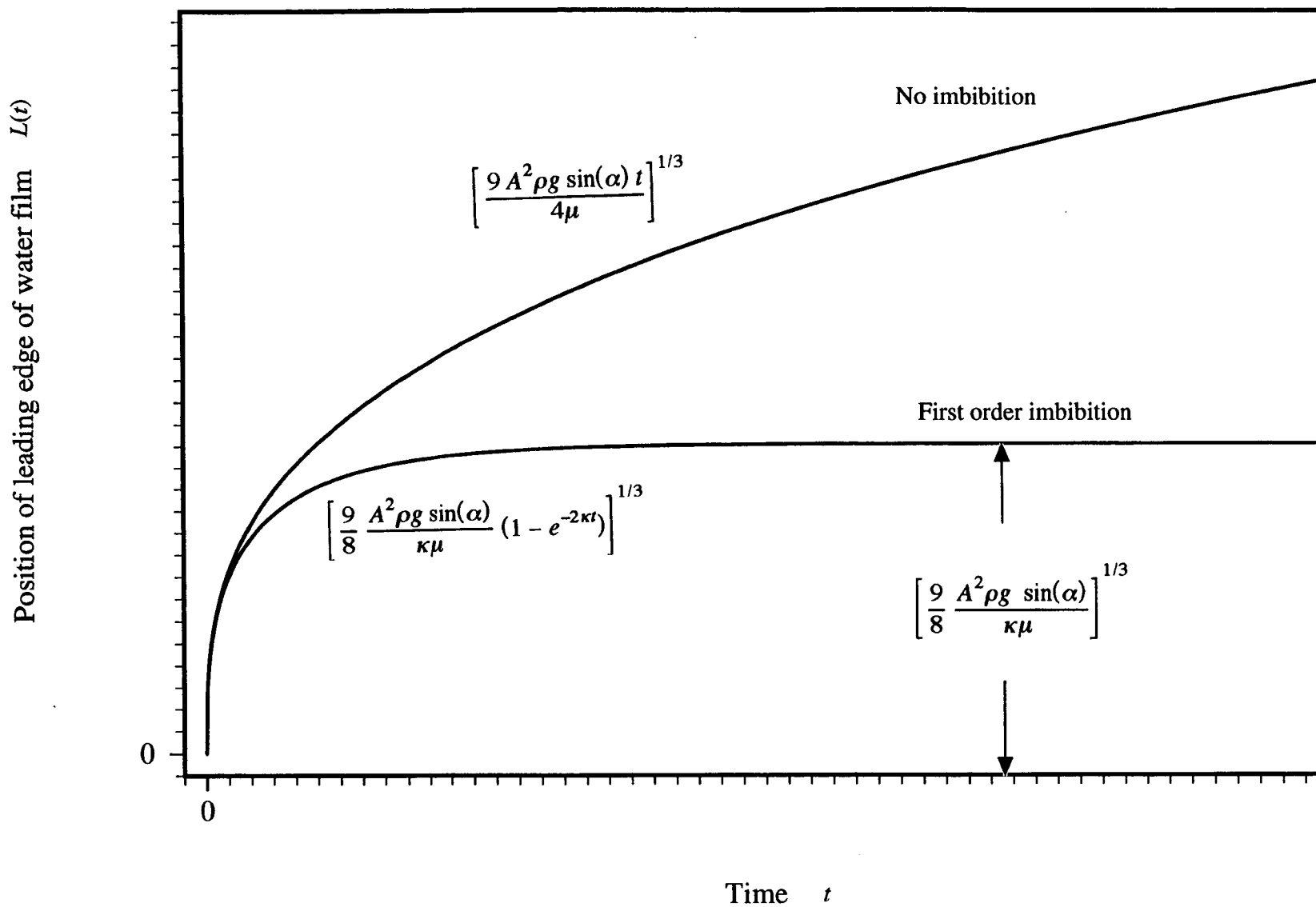


Figure 3-3. Position of leading edge of water film: comparison of first order imbibition and zero imbibition

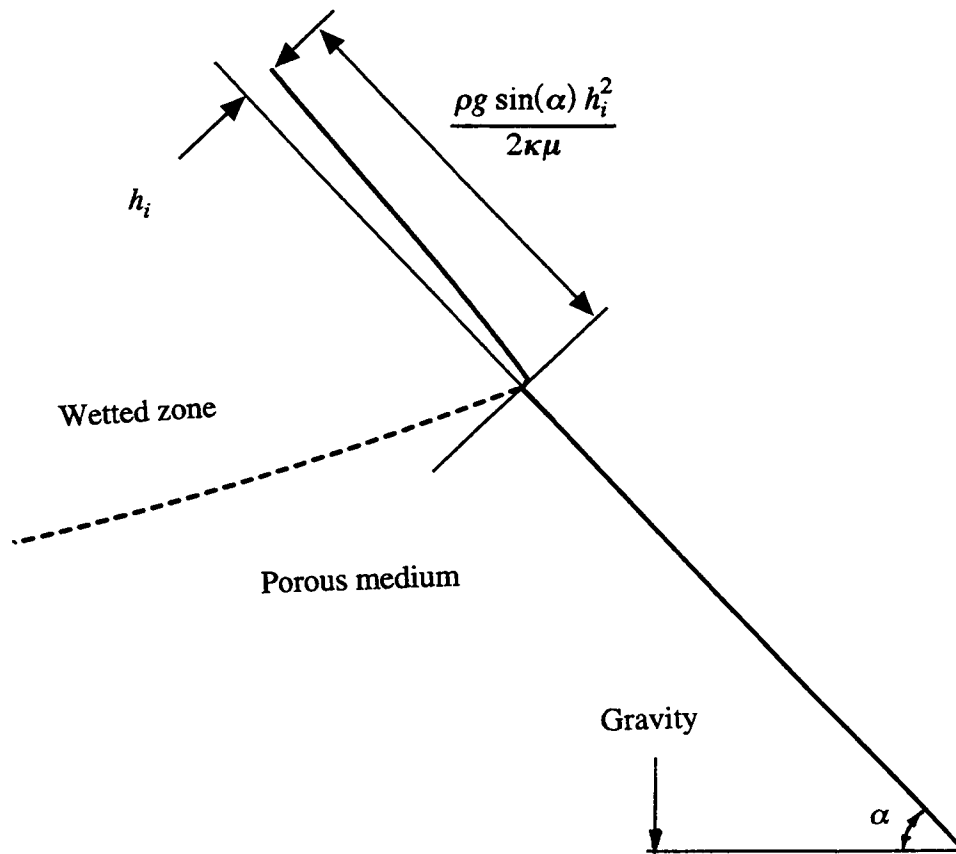


Figure 3-4. Penetration length of water under Dirichlet upstream boundary condition with first order imbibition

$$\begin{aligned} \tilde{h}_i &= \frac{h_i^n + h_{i-1}^n}{2} - \frac{\Delta t}{2\Delta x} (G_{i+1}^n - G_i^n) \\ \hat{h}_i &= \tilde{h}_i - \frac{\Delta t}{\Delta x} (\tilde{G}_i - \tilde{G}_{i-1}) \\ h_i^{n+1} &= \hat{h}_i + s\Delta t \end{aligned} \quad (3-13)$$

where $G = ch^3/3$, h_i^n is the numerically approximated value of the height of the thin-film at the i th node at the n th time-step, Δx and Δt are the spatial and temporal discretization intervals, and s is the fluid flux as defined in Eq. (2-9a). This numerical scheme is adapted from Peyret and Taylor (1983). The first two steps solve the thin-film equation without any loss term. The averaging of the head incorporated in the first step is chosen because the direction of movement of the front of water in this analysis is in the direction of increasing i . This averaging was found to be critical in obtaining solutions without spurious

oscillations. The time step Δt needs to be smaller than $\Delta x/ch^2$ by the Courant-Fredrichs-Lewy (CFL) condition, to solve the thin-film equation without any water loss. The third step incorporates the water loss term. The time step needs to be appropriately small to temporally resolve the imbibition process. It is chosen so that the water body does not lose more than half a percent of its initial maximum height in a time step, for the maximum possible imbibition in the time step. The spatial discretization is primarily based on the original dimensions of the water introduced on the plane. As the mechanism by which water is introduced onto the porous medium is not simulated here, for convenience, the initial condition for the film height is taken to be half a sine wave in front of the origin in the following simulations.

3.2.1 Zero Imbibition

Without any imbibition, the numerical solution is compared with the large-time analytical similarity solution presented in Eqs. (3-10) and (3-11). The almost perfect fit at large times shown in Figure 3-5a is a verification of the appropriateness of the numerical scheme [Eq. (3-13)] employed here, and the well known similarity solution for a thin-film of water moving down an impervious slope [Eqs. (3-10) and (3-11)]. The ability of the numerical approximations to capture the sharp front accurately was tested for large travel distances compared to the initial longitudinal dimensions of the water body. The averaging of the head performed in the first step of the numerical scheme [Eq. (3-13)] avoids spurious oscillations at the front tip, but does not dampen the solution in any detrimental way.

An interesting feature observed in the numerical solution at early times is the adjustment of the shape of the water body. For the initial conditions employed here, that is, half a sine wave, the front end steepens to form a sharp front before it moves ahead. Although, in terms of water mass, there is a movement of the water center of gravity forward, the dimension of contact with the solid surface remains constant for a while. Such waiting-time solutions on impervious surfaces have been previously presented by Tayler (1986).

3.2.2 First Order Imbibition

A first order loss term is introduced in the numerical solution and a comparison made with the derived similarity solution, in Figure 3-5b. The new similarity solution presented here [Figure 3-6a, and Eqs. (3-4), (3-5), (3-6), (3-9)] for a thin layer of water moving down a porous slope, and losing water at a rate proportional to the height of water, is the correct large time solution to Eq. (2-9a). The penetration length as a function of the system parameters was found to be adequately predicted by the simple expression Eq. (3-7). The condition for the applicability of the similarity solution derived here is worth repeating. If the water loss process is slow enough that the mass of water travels down the porous incline distances comparable to its original dimensions, the analytical expressions presented in Section 3.1 apply. This assumption excludes the case in which the water height rapidly decays to zero without any movement, which of course can be simulated by solving the ordinary differential equation resulting from neglecting the transport term in the thin-film Eq. (2-9a).

3.2.3 Green-Ampt Imbibition

In this representation of flow in an unsaturated porous medium, imbibition takes place as a sharp front of distinct moisture content (Figure 3-6a). Additionally, it is assumed here that imbibition of water into the porous medium takes place orthogonal to the porous plane due to a diffusive flux (driven by capillary forces inside the porous medium). The sink term to the thin-film equation is given by

45 degree incline

3-10

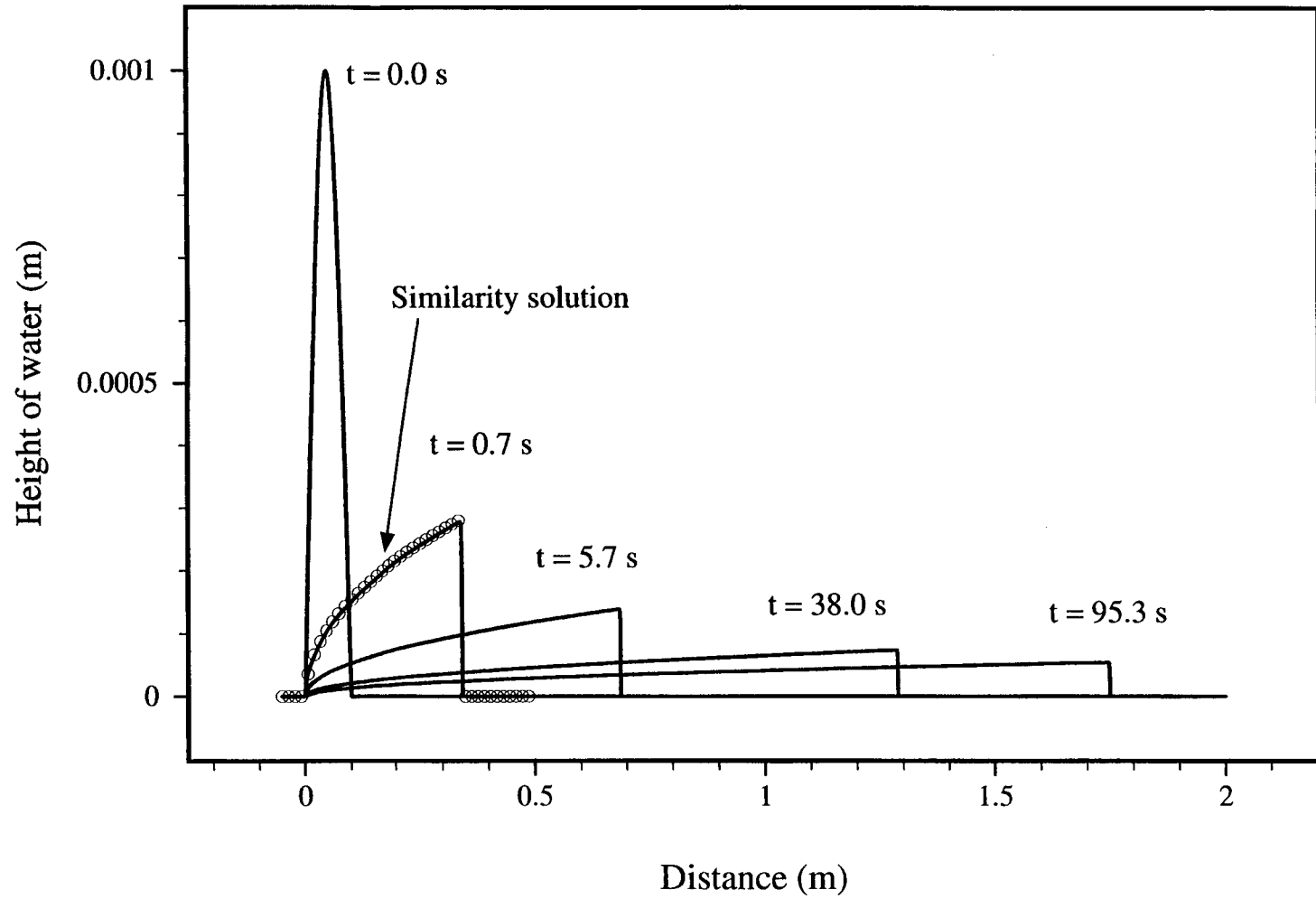
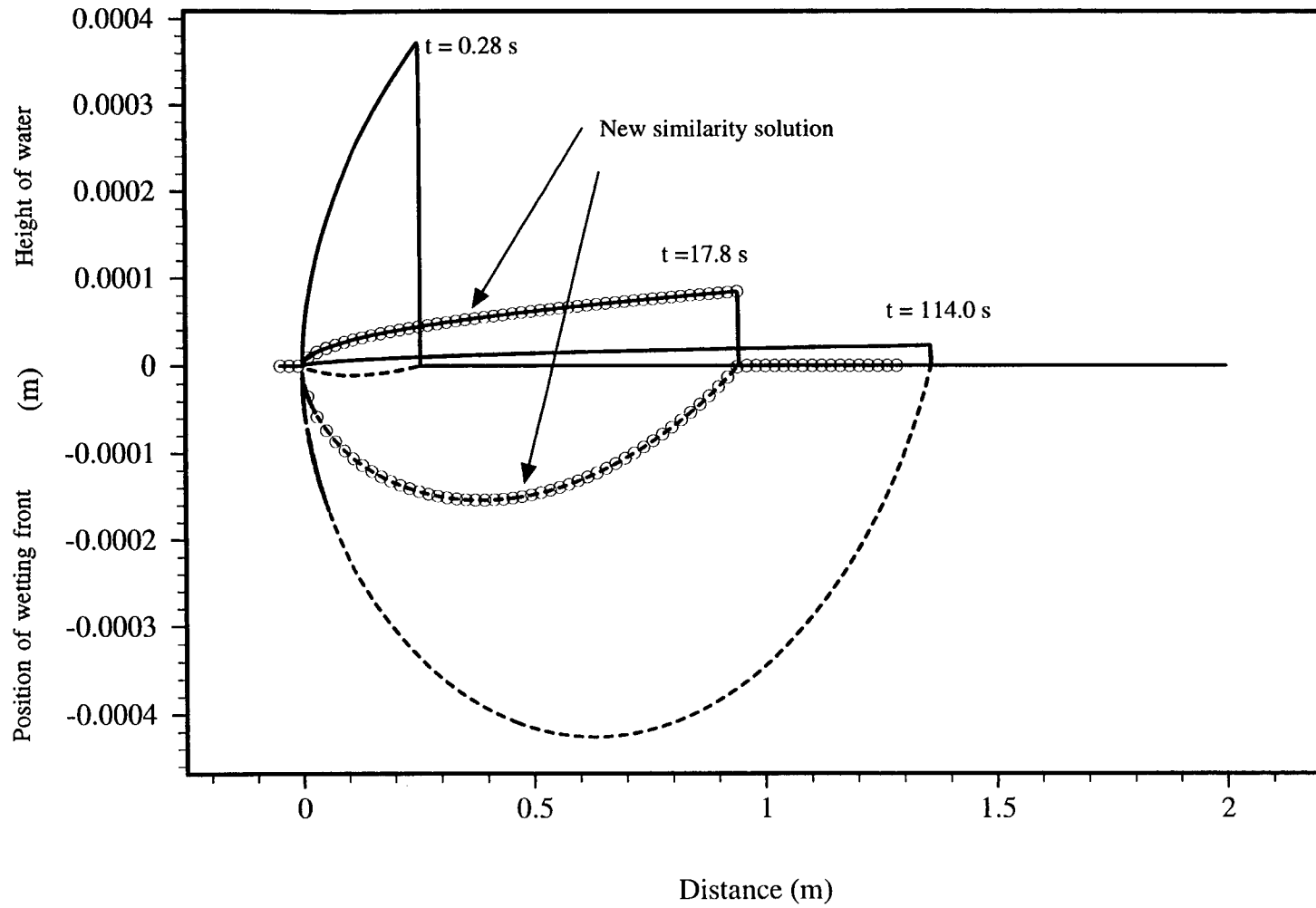


Figure 3-5a. Numerical approximation for thin-film flow: comparison with similarity solution for zero imbibition

45 degree incline



3-11

Figure 3-5b. Numerical approximation for thin-film flow: comparison with new similarity solution for first order imbibition

$$s(x_1, t) = -K_{GA} \frac{[h(x_1, t) \cos(\alpha) + \psi_f]}{Z_f(x_1, t)} I[h(x_1, t)] \quad (3-14a)$$

where $I[h(x_1, t)]$, an indicator function takes a value zero when $h=0$, and a value of 1 when $h>0$. In Eq. (3-14a), Z_f is the distance of the wetting front from the interface, K_{GA} is the hydraulic conductivity and ψ_f is the suction head ahead of the wetting front. For θ_w , the wetted zone moisture content, and θ_b , the initial moisture content, the velocity of the wetting front inside the porous medium is given by

$$\frac{dZ_f(x_1, t)}{dt} = \frac{K_{GA}[h(x_1, t) \cos(\alpha) + \psi_f]}{(\theta_w - \theta_b)Z_f(x_1, t)} I[h(x_1, t)] \quad (3-14b)$$

When the height of water at a point becomes zero, the sink term is set to zero. The moisture front inside the porous medium is tracked only as long as there is a nonzero height of water outside. Equation (3-14b) can be rewritten as

$$Z_f(x_1, t) = \left[\frac{2K_{GA}}{(\theta_w - \theta_b)} \left(\int_0^t \{h(x_1, \tau) \cos(\alpha) + I[h(x_1, \tau)] \psi_f\} d\tau \right) \right]^{1/2} \quad (3-15)$$

Equations (3-14a) and (3-15) are easily coupled to the numerical scheme [Eq. (3-13)] to solve for the thin-film flow, by evaluating the integral Eq. (3-15) numerically. In this work, K_{GA} , θ_w , and θ_b are assumed to be constant, and $Z_f(x_1, 0) = 0$.

The effect of gravity on water inside a porous medium of extremely small permeability can be expected to be much smaller than that on water outside it. In this adaptation of the Green-Ampt (1911) model the impact of gravity on water inside the porous medium is being neglected. The flux of moisture inside the porous medium associated with gradients in moisture content in the x_1 direction is also being neglected. Further simplification is achieved if we assume that the suction head ahead of the wetting front is much larger than the height of the thin-film

$$\frac{\psi_f}{h \cos(\alpha)} \gg 1 \Rightarrow s = - \sqrt{\frac{D_{GA}}{T(x_1, t)}} I[h(x_1, t)] \quad (3-16a)$$

where D_{GA} , the "imbibition coefficient" is given by

$$D_{GA} = \frac{K_{GA}(\theta_w - \theta_b)\psi_f}{2} \quad (3-16b)$$

and T is the duration of ponding at a point

$$T(x_1, t) = \int_0^t I[h(x_1, \tau)] d\tau \quad (3-16c)$$

Correspondingly, the distance of the wetting front away from the interface is given by

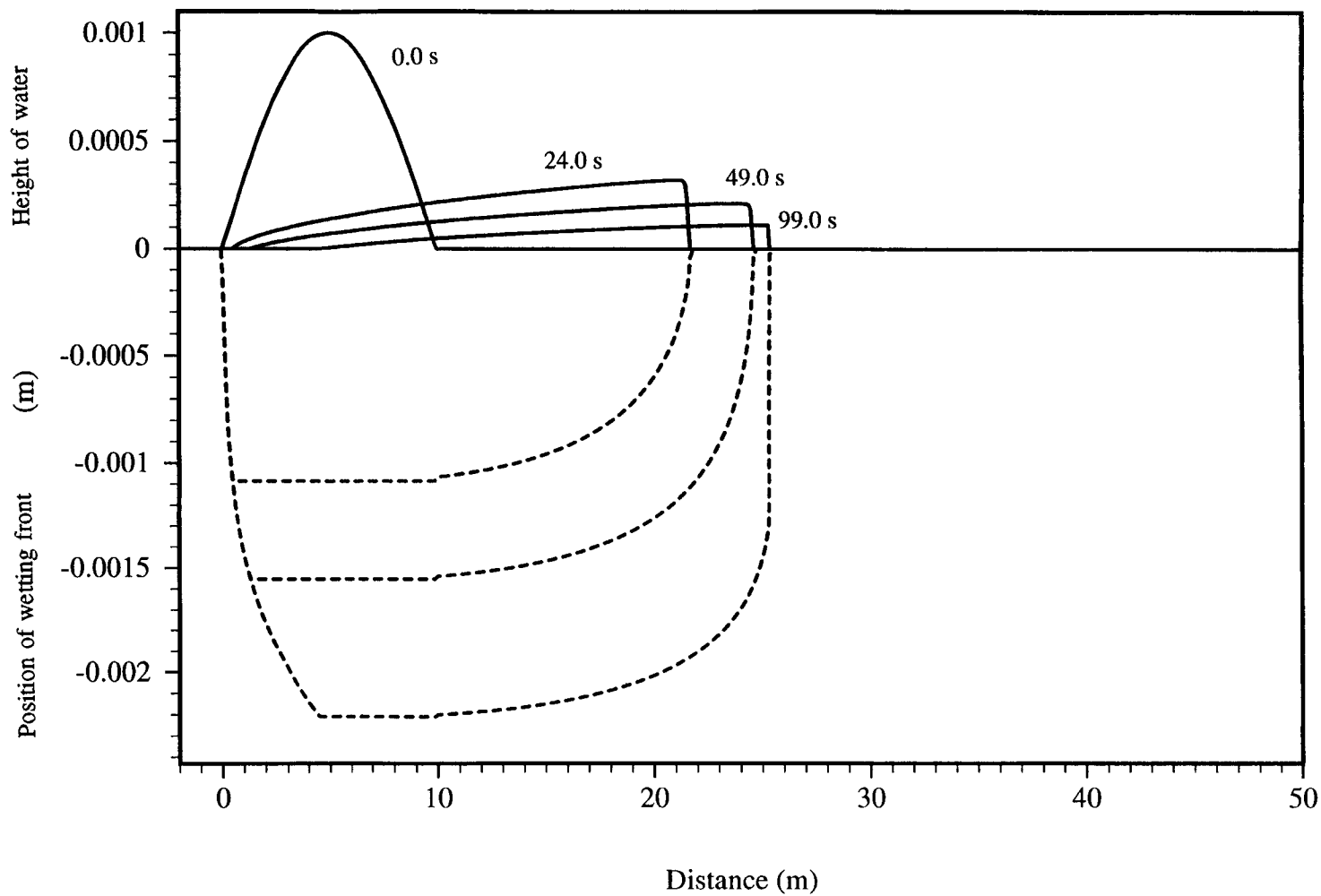
$$Z_f(x, t) = \frac{\sqrt{4D_{GA}T(x_1, t)}}{\theta_w - \theta_b} \quad (3-16d)$$

Philip (1969) presents a detailed account of such an unsaturated flow representation. The numerical results shown here use Eq. (3-16) as the imbibition model. A specification of D_{GA} is all that is needed to incorporate the rate of imbibition of water into porous medium in this simplified model. The spatial temporal evolution of the thin layer of water and the wetting front inside the porous matrix is shown in Figure 3-6a, with $D_{GA} = 1.00 \times 10^{-10} \text{ m}^2/\text{s}$. The difference between the background moisture content and that of the wetted zone, that is, $\theta_w - \theta_b$, is 0.1.

The film of water introduced onto the porous medium flattens and forms a sharp front as it moves down the unsaturated porous incline. The gravity and viscosity effects cause the rear end to be thinner than the front. Imbibition further reduces the height of the water film and the rear limit of nonzero height of water advances and catches up with the front as the flow-imbibition process proceeds. The maximum distance to which the front end of the water body is able to move is the penetration length. The kink in the plot showing the position of the wetting front (Figure 3-6a) is due to the initial adjustment of the shape of the water on the porous medium. For a short period of time, the dimensions of contact between the water and porous medium remain constant. During that time, the wetting front in the porous medium, beneath the layer of water, moves away from the interface according to Eq. (3-16d). The locations of the front and rear ends of the water body are shown in Figure 3-6b. The effect of reducing the initial amount of water applied by reducing the maximum initial height of the water is shown in Figure 3-6c. If the initial thickness of the film is small enough so that the time over which the film adjusts its shape is greater than the time required for it to be completely imbibed, there may be no downward movement of water outside the porous matrix, as shown in Figure 3-6c. The effect of changing the angle of inclination of the unsaturated porous incline is shown in Figure 3-6d. The film travels further but gets imbibed faster as the rate at which the water body encounters dry porous medium is also greater. This negative feedback diminishes the sensitivity of the penetration length to the angle of inclination. The larger the imbibition coefficient, the more intense is this negative feedback effect. A decrease in the imbibition coefficient makes the water move much further, as shown in Figure 3-6e.

Like the first order imbibition case, the leading edge of water cannot travel beyond a distinct maximum value (the penetration length). The leading edge does show a little recession at later times

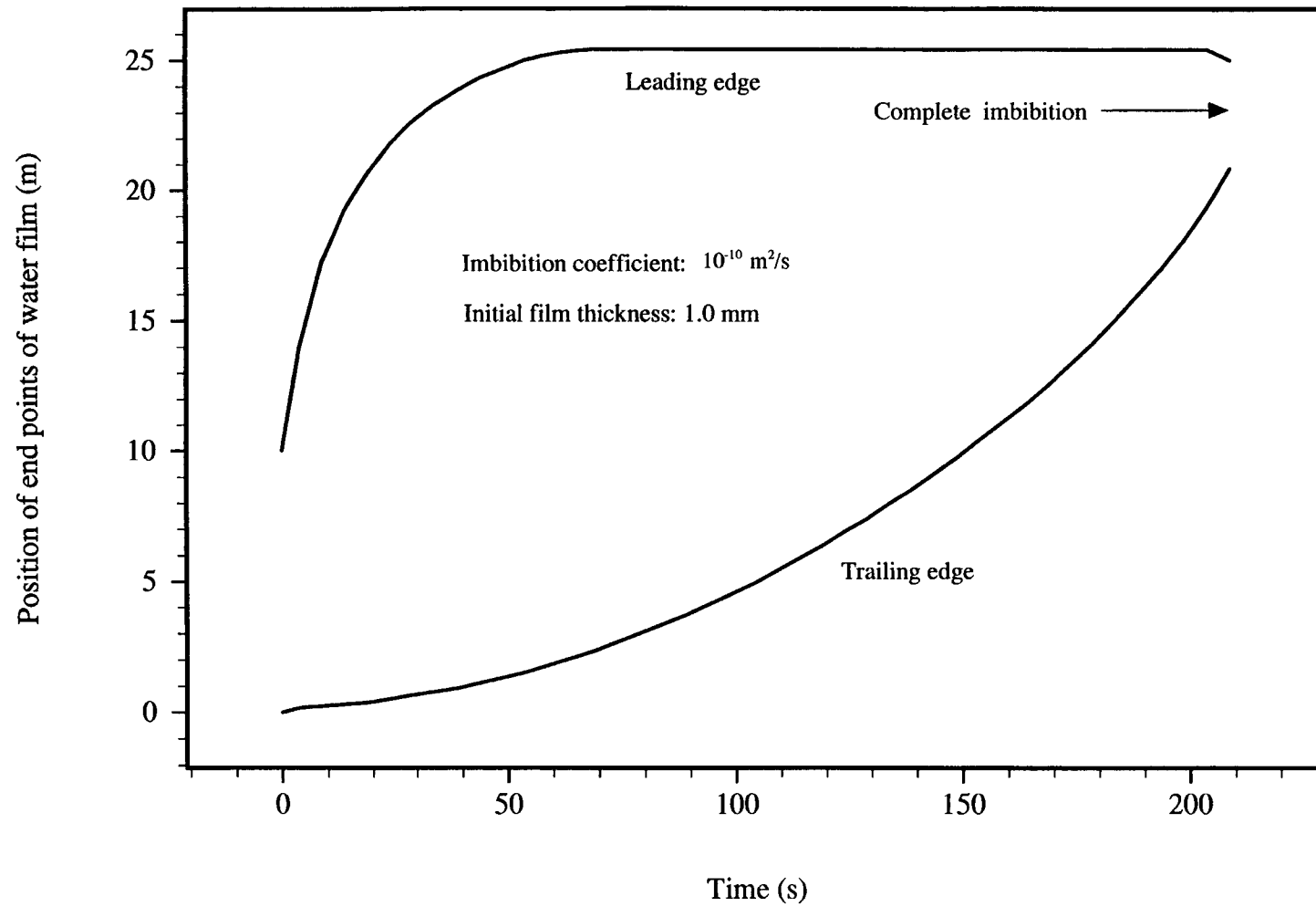
45 degree incline



3-14

Figure 3-6a. Numerical approximation of thin-film flow with Green-Ampt imbibition: evolution of water film and wetting front inside the porous medium

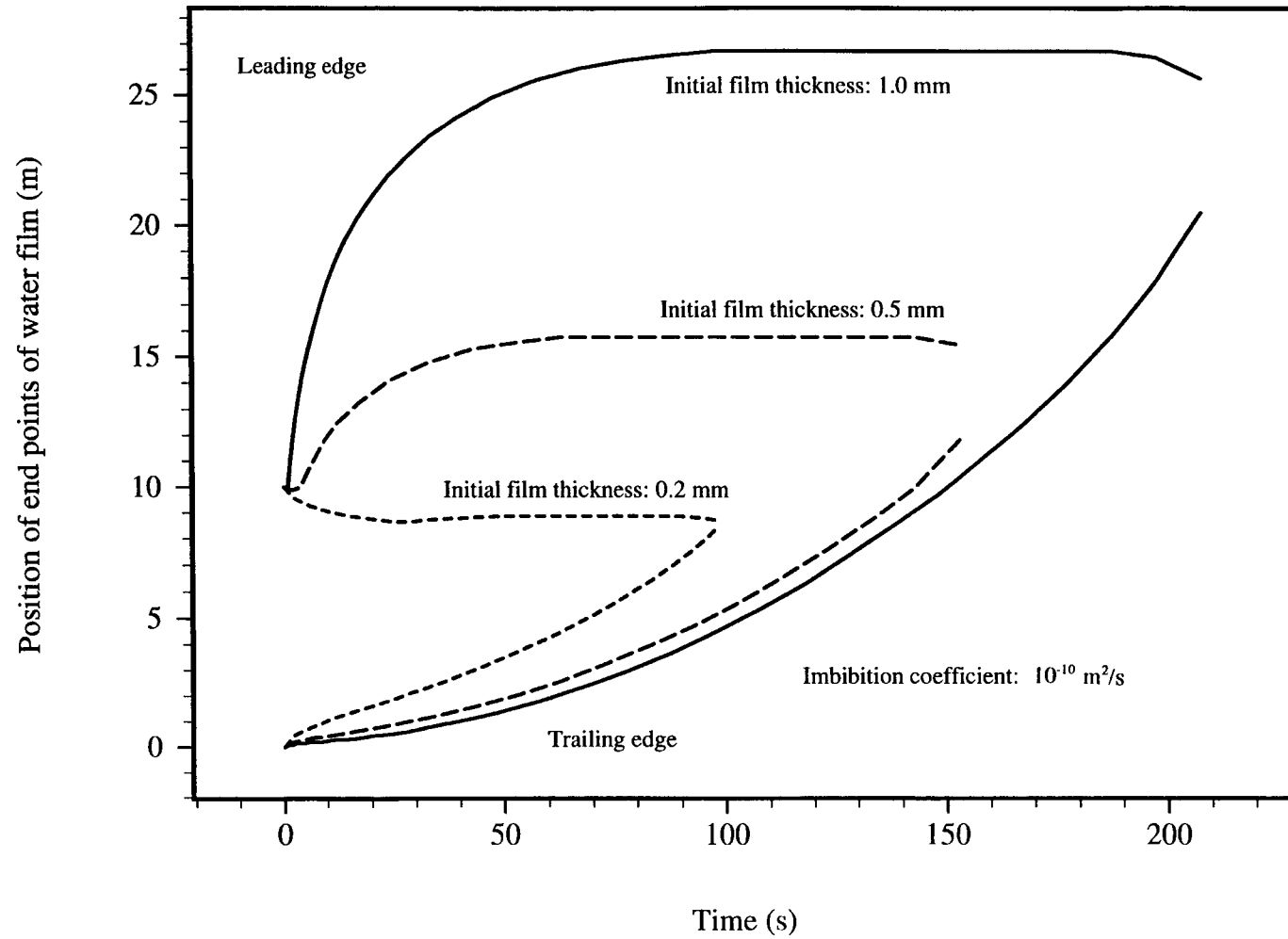
45 degree incline



3-15

Figure 3-6b. Numerical approximation of thin-film flow with Green-Ampt imbibition: end points of water film

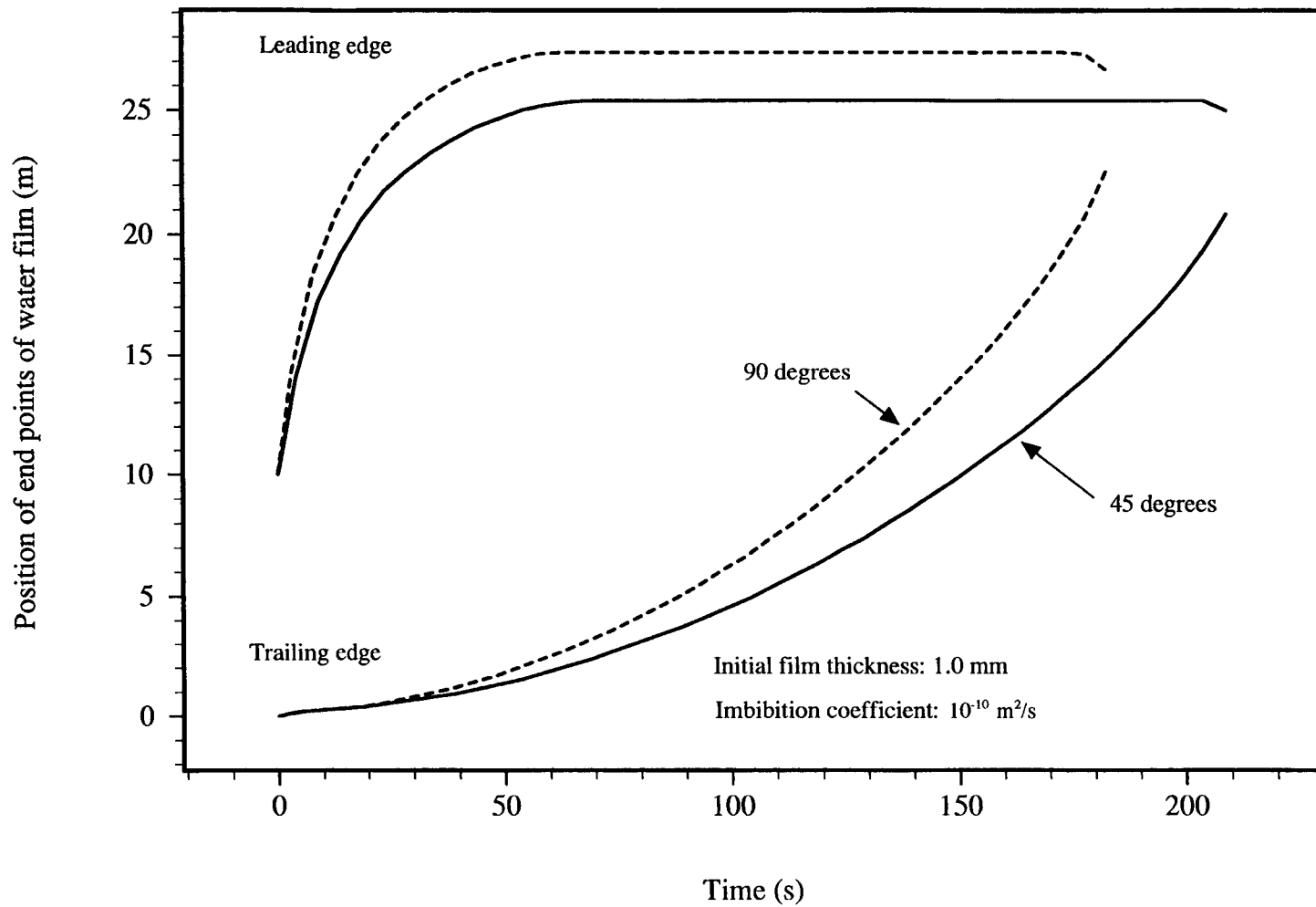
45 degree incline



3-16

Figure 3-6c. Numerical approximation of thin-film flow with Green-Ampt imbibition: effect of varying initial height of water film

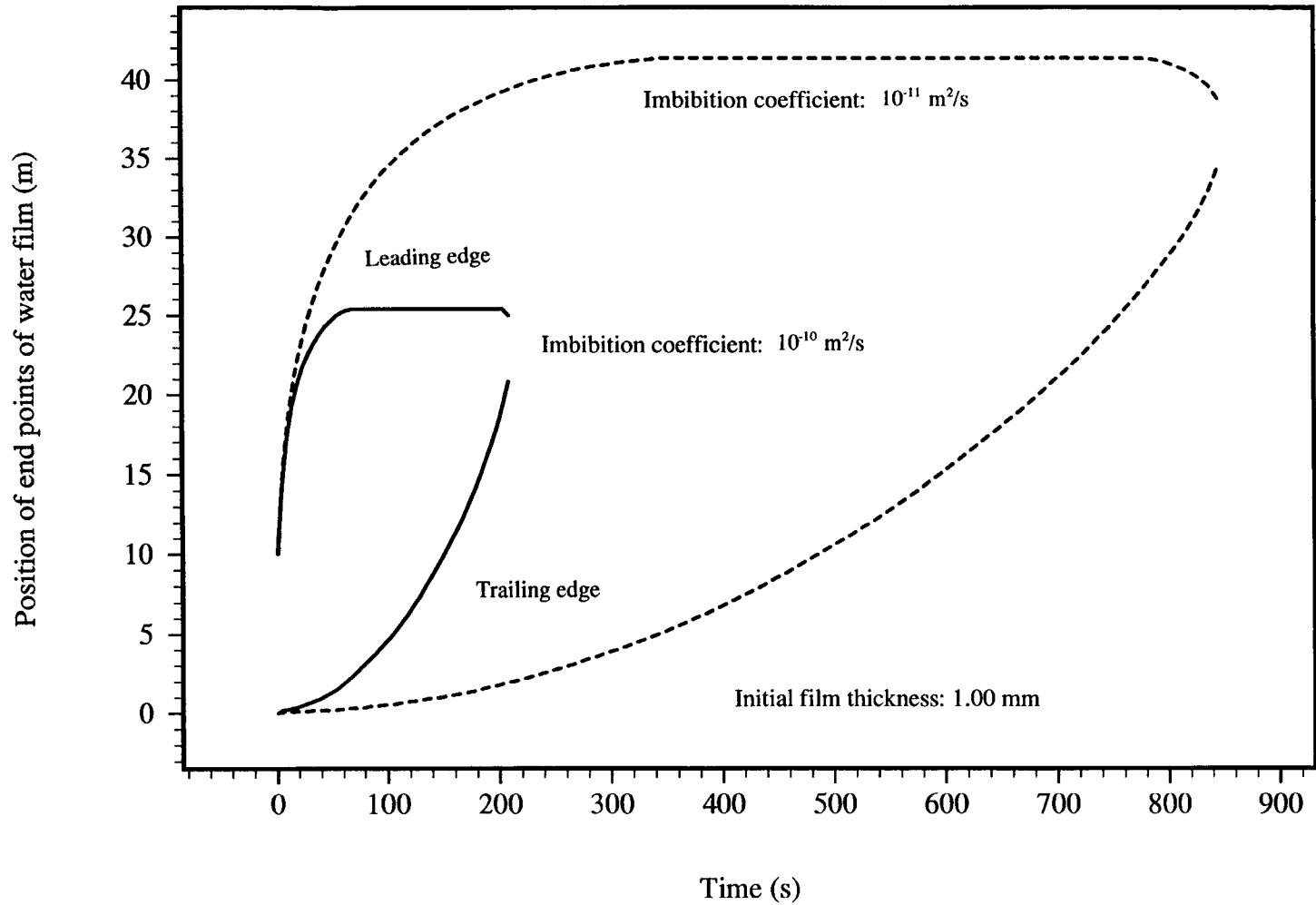
45 and 90 degree inclines



3-17

Figure 3-6d. Numerical approximation of thin-film flow with Green-Ampt imbibition: effect of changing angle of inclination

45 degree incline



3-18

Figure 3-6e. Numerical approximation of thin-film flow with Green-Ampt imbibition: effect of changing Green-Ampt imbibition coefficient

because it is in the zone of maximum imbibition rate as the wetting front is relatively shallow. In contrast to the first order imbibition case, the rear limit of the water body advances with time. This advance occurs because the Green-Ampt imbibition can completely deplete the water at a point, unlike the first order loss case. The rear end of the water body advances and catches up with the leading edge at the instant water is completely imbibed into the porous medium. The feature of the rate of imbibition decaying with time due to the decreasing suction gradient [Eqs. (3-16a) and (3-16c)] is important. Consequently, for a Dirichlet upstream boundary condition, there is no finite penetration length for the Green-Ampt imbibition model, unlike the first order loss case [Figure 3-4, Eq. (3-12)].

In the numerical results presented here, the mass loss errors at the time of complete imbibition were extremely small. For each of the results shown in Figures 3-6a through 3-6e, the numerically approximated dependent variables became insensitive to numerical discretization intervals at the level of discretization employed. In coupling the thin-film evolution to the Green-Ampt model-based imbibition of water into the porous medium, the coupling of distinct fluid flow phenomenon with distinct characteristic time-scales has been accomplished. The next section reports a numerical model coupling the thin-film flow to 2D-Richards' equation-based unsaturated flow.

4 THIN-FILM FLOW WITH RICHARDS' EQUATION-BASED IMBIBITION

4.1 NUMERICAL APPROXIMATION FOR VARIABLY SATURATED FLOW

The flow inside the porous medium governed by Eq. (2-4) is solved by an explicit two-step predictor-corrector scheme due to MacCormack (1969), modified to take into account the nonlinear coefficient multiplying the time derivative term. The MacCormack (1969) scheme is discussed by Peyret and Taylor (1983). Consider a general nonlinear advection-diffusion equation with nonlinear coefficients;

$$\beta(f) \frac{\partial f}{\partial t} + \sum_{m=1}^2 \left\{ \frac{\partial}{\partial x_m} \left[F_m(f) - \xi(f) \frac{\partial f}{\partial x_m} \right] \right\} = 0 \quad (4-1)$$

The corresponding terms in Richards' equations are easily obtained by comparing Eqs. (2-4) and (4-1). The two-step finite-difference scheme adopted in this work is

$$\tilde{f}(i,j) = f^n(i,j) - \frac{\Delta t}{\beta[f^n(i,j)]} \sum_{m=1}^2 \Delta_{x_m}^+ \left\{ F_m[f^n(i,j)] - N_m(i,j) \Delta_{x_m}^- f^n(i,j) \right\} \quad (4-2a)$$

$$f^{n+1}(i,j) = \frac{1}{2} [f^n(i,j) + \tilde{f}(i,j)] - \frac{\left(\frac{\Delta t}{2}\right)}{\beta \left[\frac{1}{2} \{f^n(i,j) + \tilde{f}(i,j)\} \right]} \sum_{m=1}^2 \Delta_{x_m}^- \left\{ F_m[\tilde{f}(i,j)] - \tilde{N}_m(i,j) \Delta_{x_m}^+ \tilde{f}(i,j) \right\} \quad (4-2b)$$

where

$$\begin{aligned}
 N_1(i,j) &= \frac{1}{2} \{ \xi [f^n(i,j)] + \xi [f^n(i-1,j)] \} \\
 N_2(i,j) &= \frac{1}{2} \{ \xi [f^n(i,j)] + \xi [f^n(i,j-1)] \} \\
 \tilde{N}_1(i,j) &= \frac{1}{2} \{ \xi [\tilde{f}(i,j)] + \xi [\tilde{f}(i+1,j)] \} \\
 \tilde{N}_2(i,j) &= \frac{1}{2} \{ \xi [\tilde{f}(i,j)] + \xi [\tilde{f}(i,j+1)] \}
 \end{aligned}
 \tag{4-2c}$$

and $\Delta_{x_m}^+$ and $\Delta_{x_m}^-$ are the forward and backward finite difference operators in the m th direction, respectively.

The spatial discretization in the m th direction, Δ_{x_m} , is chosen so that the implied grid Peclet number is less than one in both directions; that is

$$Pg_m \equiv \frac{\Delta_{x_m} \left| \frac{\partial F_m}{\partial f} \right|}{2\xi} < 1
 \tag{4-3a}$$

for $m=1$ and 2 . The time step Δt is chosen based on numerical stability considerations (Peyret and Taylor, 1983),

$$\Delta t < \frac{\beta \Delta_{x_m}^2}{4\xi + \left(\left| \frac{\partial F_1}{\partial f} \right| + \left| \frac{\partial F_2}{\partial f} \right| \right) \Delta_{x_m}}
 \tag{4-3b}$$

These two conditions, along with adequate discretization of initial conditions, were the selected spatial-temporal discretization criteria. Finlayson (1985) provides a detailed account of spatial-temporal discretization criterion for Richards' equation. For the simulations reported here, the grid Peclet number was always less than 0.1, and the time step was taken to be less than half the maximum allowed for stability considerations [Eq. (4-3b)]. The moisture content is advanced in time by a two-step predictor-corrector method

$$\begin{aligned}\bar{\theta}(i,j) &= \theta^n(i,j) - S [\psi^n(i,j)] \{\Psi(i,j) - \psi^n(i,j)\} \\ \theta^{n+1}(i,j) &= \frac{\theta^n(i,j) + \bar{\theta}(i,j)}{2} - S \left[\frac{\psi^n(i,j) + \Psi(i,j)}{2} \right] \\ &\quad \left\{ \psi^{n+1}(i,j) - \frac{\psi^n(i,j) + \Psi(i,j)}{2} \right\}\end{aligned}\quad (4-4)$$

where S is as previously defined in Eq. (2-4b).

The performance of this simple methodology and discretization criteria to find a numerical solution for variably saturated flow in porous medium is assessed by comparing it with a transient analytical solution for Burgers' (1974) equation

$$\frac{\partial f}{\partial t} + \frac{\partial}{\partial x} \left(\frac{f^2}{2} - \xi \frac{\partial f}{\partial x} \right) = 0 \quad (4-5)$$

Solutions to Eq. (4-5) can be used to represent infiltration with some special representations of the hydraulic conductivity-moisture content relationship (Philip, 1974; Clothier and White, 1981; Clothier et al., 1981; Rogers and Ames, 1989). The analytical solution due to Whitham (1974)

$$f(x,t) = \frac{\frac{8\pi\xi}{\lambda} \sum_{n=1}^{\infty} n \exp \left[-\frac{4\pi^2 n^2 \xi \left(t + \frac{\pi}{16} \right)}{\lambda^2} \right] \sin \left(\frac{2\pi n x}{\lambda} \right)}{1 + 2 \sum_{n=1}^{\infty} \exp \left[-\frac{4\pi^2 n^2 \xi \left(t + \frac{\pi}{16} \right)}{\lambda^2} \right] \cos \left(\frac{2\pi n x}{\lambda} \right)} \quad (4-6)$$

is compared with the solution obtained from the numerical approximation [Eq. (4-2)]. The initial and boundary conditions correspond to Eq. (4-6) with $t=0$ and $x=0$ and λ , respectively. In Figure 4-1a, the results shown are for $\xi=1$, domain length $\lambda=1$, and numerical spatial discretization $\Delta x=0.05$, implying a grid Peclet number less than one, with a time step satisfying the stability criteria [Eq. (4-3b)]. These two criteria [Eqs. (4-3a) and (4-3b)] and an adequate resolution of initial conditions produced favorable comparisons. Of course, as ξ is reduced, a smaller grid is required to get accurate solutions, and the time step required for stability becomes smaller.

The second check of the adopted numerical technique [Eq. (4-2)] is by comparing the steady-state solution of Eq. (2-4) with a Gardner (1958) hydraulic conductivity function, that is,

$K(\psi) = K_s \exp(-\alpha_g \psi)$, $\psi \geq 0$. Following Gardner (1958) and Bear (1972), for Dirichlet boundary conditions, it can be shown

$$\psi(z) = \psi(0) - \frac{1}{\alpha_g} \ln \left[1 - \frac{\{1 - e^{\alpha_g[\psi(0) - \psi(H)]}\}}{(1 - e^{\alpha_g H})} (1 - e^{\alpha_g z}) \right] \quad (4-7)$$

For a specified flux q at $z=0$ and specified head boundary condition at $z = H$

$$\psi(z) = \psi(H) + \frac{1}{\alpha_g} \ln \left\{ \frac{K_s e^{-\alpha_g[\psi(H) - H]}}{K_s e^{-\alpha_g[\psi(H) - z]} + q(e^{\alpha_g H} - e^{\alpha_g z})} \right\} \quad (4-8)$$

Both of these solutions are valid as long as the suction head $\psi = -p/\rho g$ is positive throughout the domain. However, such solutions can be extended to the case where parts of the domain are completely saturated. In both of these solutions, z is positive downwards (aligned with gravity), and varies from 0 to H . For $K_s = 10^{-4}$ m/s, $\alpha_g = 0.1 \text{ m}^{-1}$, $H = 10$ m, with spatial discretization of 0.05 m, Figure 4-1b shows the comparison for the Dirichlet boundary conditions. Figure 4-1c illustrates a case with a specified flux equal to K_s applied at the $z = 0$ m, and a specified suction head of 10 m at $z = 10$ m.

In marching to steady-state, the coefficient S [Eq. (2-4c)] does not play any role in determining the steady state. However, in transient problems, the storage coefficient needs to be specified. In the porous flow problem, we can expect some portions of the domain to be completely saturated, therefore, the moisture content-suction relationship for both saturated and unsaturated conditions is needed. The function

$$\begin{aligned} \theta(\psi) &= \theta(0) - S_s \psi, & \psi \leq 0 \\ \theta(\psi) &= \theta(0) \exp \left[-(\beta \psi)^2 - \frac{S_s}{\theta(0)} \psi \right], & \psi > 0 \end{aligned} \quad (4-9)$$

yields a continuous and positive function for $S = -\frac{d\theta}{d\psi}$

$$\begin{aligned} S &= S_s, & \psi \leq 0 \\ S &= \left[S_s + 2\beta^2 \theta(0) \psi \right] \exp \left[-(\beta \psi)^2 - \frac{S_s}{\theta(0)} \psi \right], & \psi > 0 \end{aligned} \quad (4-10)$$

The parameters β and S_s may be varied to control the shape of the moisture-suction characteristic. The hydraulic conductivity was taken to be K_s for $\psi \leq 0$, and Gardner's (1958) $K_s \exp(-\alpha_g \psi)$ for $\psi > 0$. These simple hydraulic conductivity-suction-moisture content functions are only to illustrate the coupled thin-film flow and Richards' equation-based imbibition process. For a practical application with a specific

porous medium, direct measurement of these functions is needed. Paniconi and Wood (1993) took a similar approach to modify the moisture content-suction head function proposed by van Genuchten and Nielson (1985) to yield a nonzero value of S .

With hydraulic conductivity parameters identical to those in the previous two test problems, $\theta(0)=0.3$, $\beta = 0.001 \text{ m}^{-1}$, and $S_s = 10^{-5} \text{ m}^{-1}$, a transient moisture redistribution problem was solved for three different discretizations (0.2, 0.1, and 0.05 m). In this test problem, both the boundary conditions are of the no-flux type. A uniform suction of 1 m is the initial condition. The steady-state solution to this problem is a linear suction variation with height. That the transient solution has converged with respect to grid size is seen in Figure 4-1d, showing the solutions at two different time steps for three different discretizations, represented by the solid line, dashed line, and circles.

These one-dimensional (1D) transient and steady-state solutions were numerically simulated in both directions identically. These comparisons support the adequacy of the simple numerical scheme and the chosen discretization criteria. The simplicity of the MacCormack (1969) scheme and an *a priori* estimate of spatial-temporal discretization needs [Eqs. (4-3a) and (4-3b)] and its satisfactory performance for a few analytically tractable cases are the reasons it was chosen for this study. Needless to say, in the past two decades, a number of different numerical schemes have been successfully employed for modeling variably saturated flow (e.g., Neuman, 1973; Baca et al., 1978; Gureghian et al., 1979; Cooley, 1983; Huyakorn and Pinder, 1983; Finlayson, 1985; Ababou and Gelhar, 1988; Celia et al., 1990; Baca and Magnuson, 1992, etc.).

4.2 COUPLED THIN-FILM VARIABLY SATURATED FLOW SIMULATION

The thin-film solution [Eq. (3-13)] is coupled to the 2D variably saturated porous medium flow. On the interface between the water and variably saturated porous medium, wherever there is a nonzero height of water, the pressure head boundary condition applied to the porous medium is $h \cos(\alpha)$. At the other points on the boundary, a no-flux boundary condition is imposed, as long as the porous medium at the boundary is not fully saturated. If a point at the interface is fully saturated, water can flow in and out of the porous medium at that point as given by

$$s(x_1, t) = - K_s \cos(\alpha) + K_s \left. \frac{\partial \psi}{\partial x_2} \right|_{x_2=0} \quad (4-11)$$

A background of uniform moisture content is assumed to be the initial condition in the porous medium. The sequence by which the solution is advanced in time is as follows: impart thin-film movement, impose boundary conditions on porous medium, calculate porous medium suction head field, compute boundary flux, impart water loss or gain in the thin-film [Eq. (4-11)], next time step. A constraint on the time step in the numerical approximation is that the height of water should not decrease by more than 0.5 percent of its initial height in any time step. The discretization of the porous medium needs to be adequate for the porous medium flow as discussed in the previous section.

The parameters for the example shown here are: $\alpha = 45$ degrees, $\theta(0) = 0.1$, $K_s = 1.00 \times 10^{-8} \text{ m/s}$, $\alpha_g = \beta = 0.05 \text{ m}^{-1}$, and $S_s = 1.00 \times 10^{-4} \text{ m}^{-1}$. The initial suction head inside the porous medium is 20 m. The isotropic and homogeneous porous medium is 1.1 m long and 0.02 m thick.

The computational domain is divided into 300 and 150 cells in the length and thickness, respectively. Water is introduced over 20 cm with an initial maximum height of 1 mm. In Figure 4-2a, which shows the temporal evolution of water, on the positive y axis is the height of the water film outside the porous medium, and on the negative y axis is the center of gravity of the moisture introduced by imbibition along the direction orthogonal to the porous surface; that is

$$W(x_1) = \frac{\int_0^{-a} [\theta(x_1, x_2, t) - \theta(x_1, x_2, 0)] x_2 dx_2}{\int_0^{-a} [\theta(x_1, x_2, t) - \theta(x_1, x_2, 0)] dx_2} \quad (4-12)$$

The porous medium extends from 0 to $-a$ along the x_2 axis, a being 0.02 m in this example. This is a convenient way to present the 2D moisture distribution inside the porous medium. The evolution of the end points of the water body are shown in Figure 4-2b. The unaccounted accumulation of water mass in the numerical simulation when the water film was completely imbibed into the porous medium was 0.5 percent of the initial water mass.

Qualitatively, the simulation with the Green-Ampt imbibition representation (Figure 3-6a) is similar to that found by solving the detailed imbibition process via Richards' equation. Both these models exhibit the initial expansion of the water mass on account of gravity, and the distinct penetration length beyond which the leading edge cannot move, and the shrinking of the longitudinal dimensions of the water body with the rear end moving forward and meeting with the front end at the end of its journey outside the porous medium. The evolution of moisture inside the porous medium after a point ceases to be ponded with water is not obtained in the Green-Ampt imbibition model, which creates the rounding of the wetting front at the rear end as it advances forward (Figure 3-6a). Of course, this similarity will break down if there is a significant influence of gravity on water inside the porous matrix (which is considered in the Richards' equation model and neglected in the Green-Ampt model adapted in Section 3.2.3) over the time it takes for water to get completely imbibed.

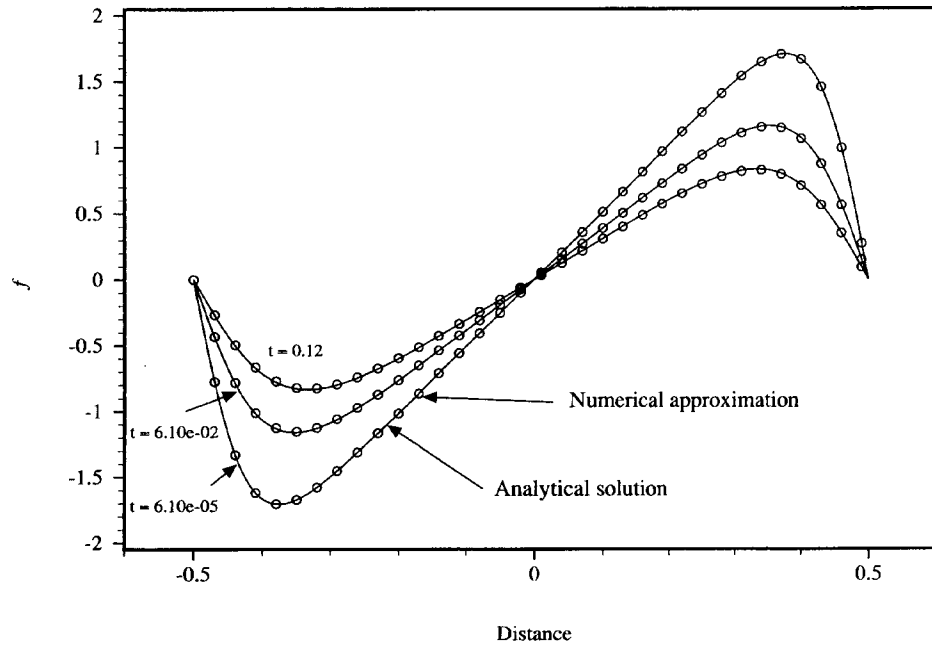


Figure 4-1a. Evaluation of a modified MacCormack (1969) scheme for unsaturated flow: comparison with transient analytical solution to Burgers' equation

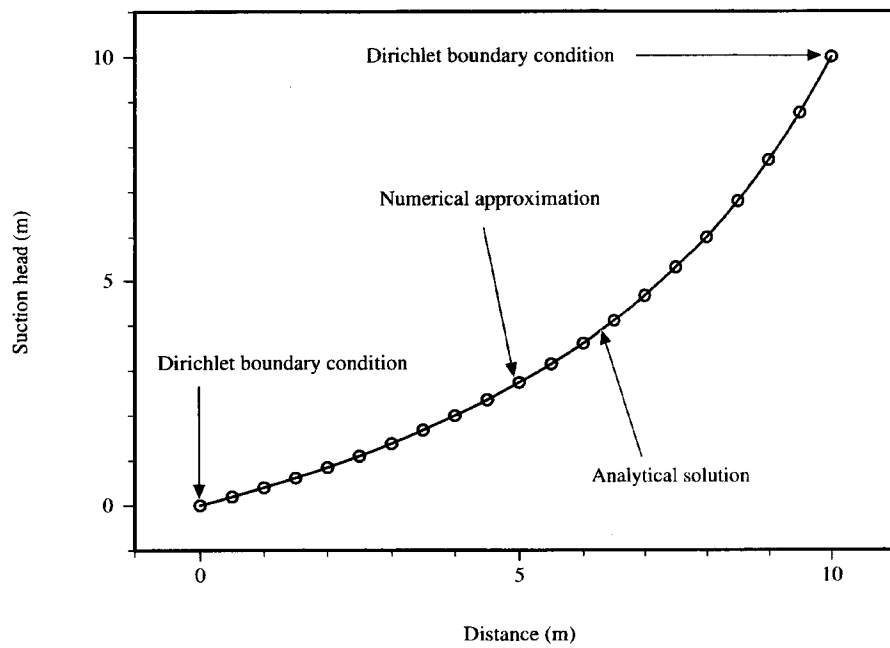


Figure 4-1b. Evaluation of a modified MacCormack (1969) scheme for unsaturated flow: comparison with steady-state analytical solution—Dirichlet boundary conditions

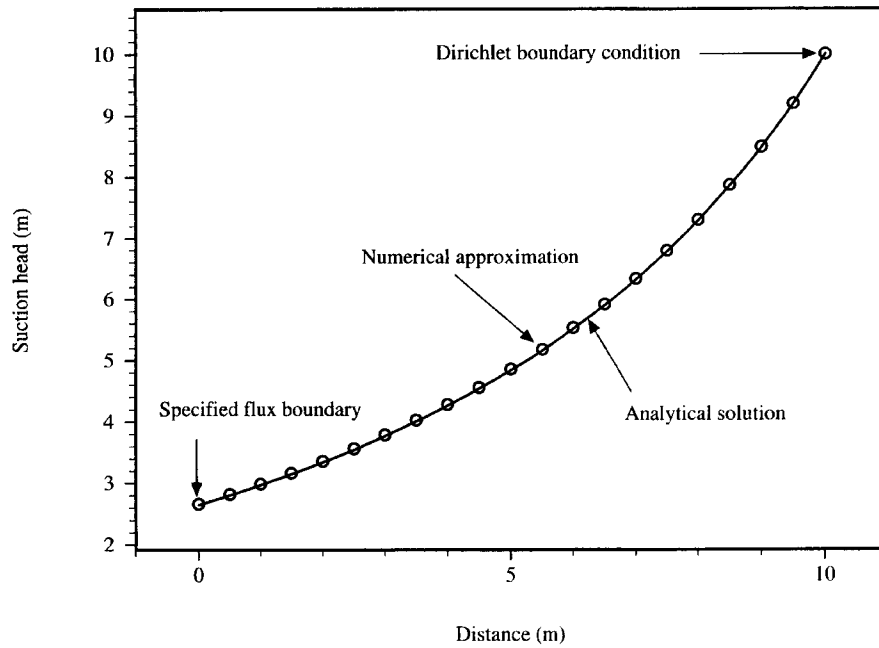


Figure 4-1c. Evaluation of a modified MacCormack (1969) scheme for unsaturated flow: comparison with steady-state analytical solution—Dirichlet and specified flux boundary condition

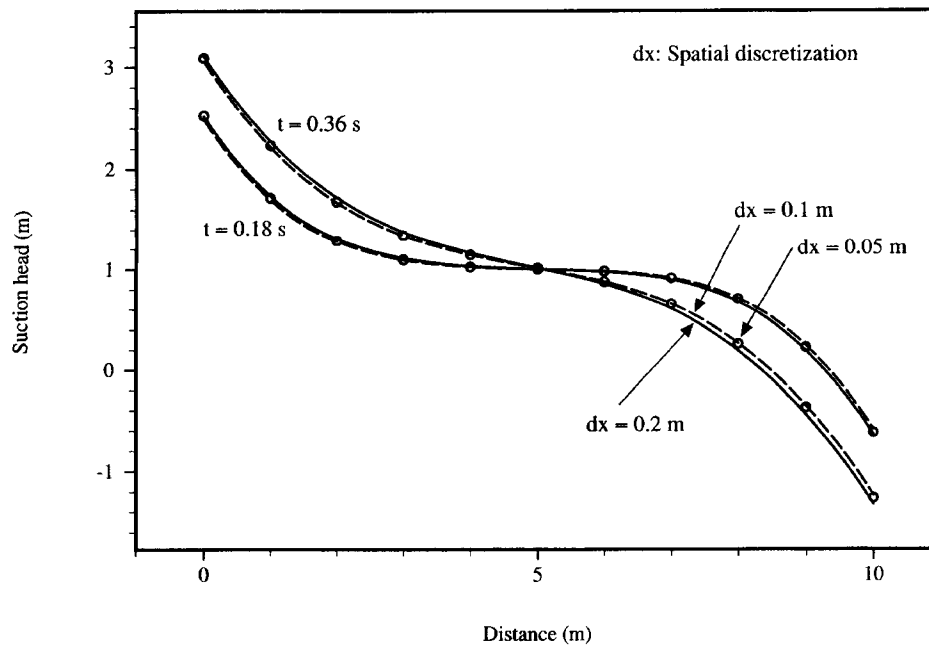
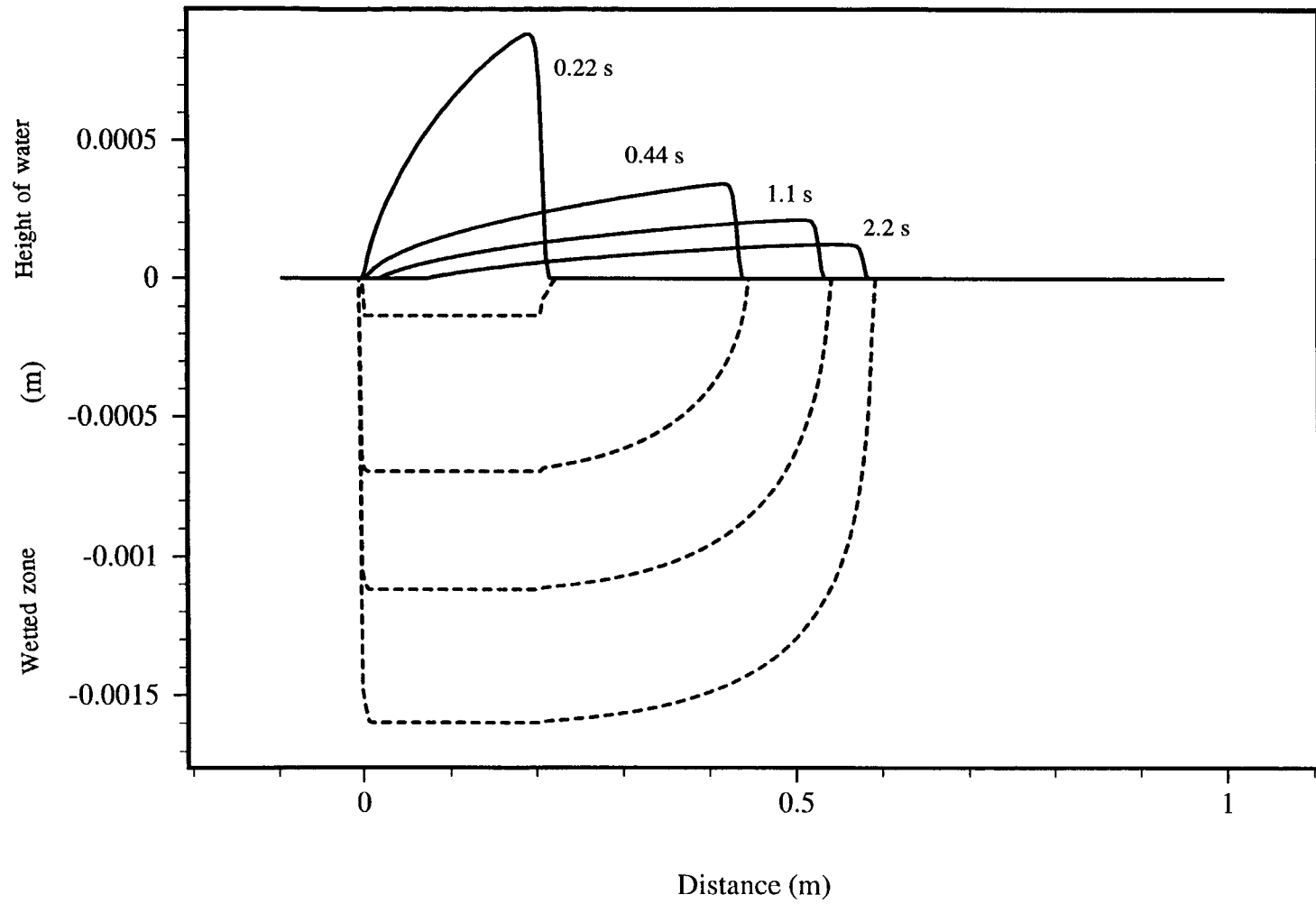


Figure 4-1d. Evaluation of a modified MacCormack (1969) scheme for unsaturated flow: convergence for transient moisture redistribution problem

45 degree incline



6-9

Figure 4-2a. Numerical approximation of coupled thin-film—Darcy imbibition: evolution of water film and wetted zone inside the porous medium

45 degree incline

4-10

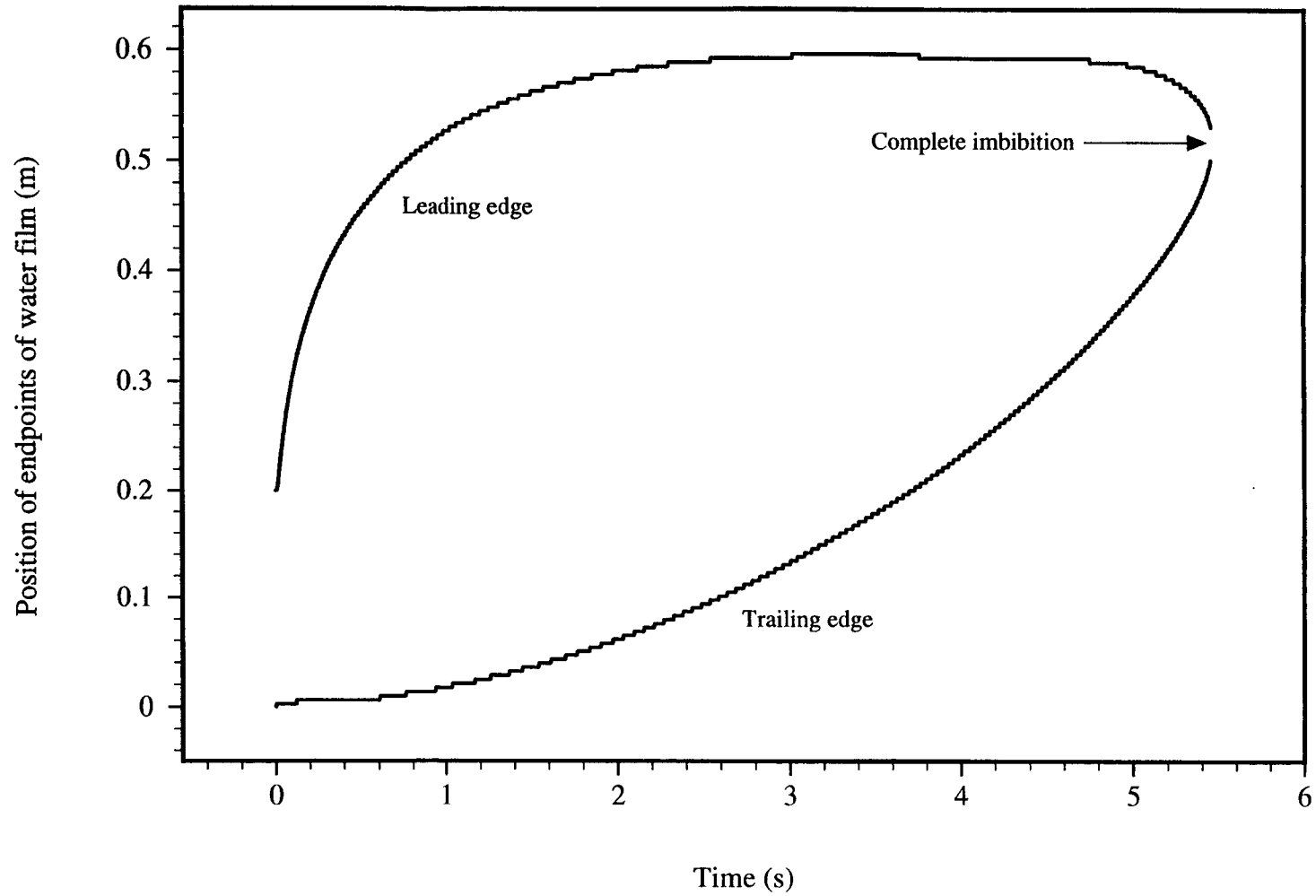


Figure 4-2b. Numerical approximation of coupled thin-film—Darcy imbibition: end points of water film

5 EXPERIMENT

The coupled viscous-unsaturated flow phenomenon, analyzed in this document, can be experimentally observed relatively simply by introducing a small quantity of water onto an unsaturated porous plane surface. For the low-permeability consolidated porous material motivating this research, determining the complete Darcy constitutive properties (i.e., hydraulic conductivity-moisture content-suction head characteristics) of the porous medium is not easy because of the large suction heads and small rates of water movement involved, and was not attempted in this study. However, the flow of water down an unsaturated plane porous incline was observed, and qualitative comparisons with model predictions were made. The value of the imbibition coefficient associated with the Green-Ampt imbibition representation (Section 3.2.3) was experimentally estimated, and quantitative predictions of the penetration length were made and compared with experimental observations.

5.1 SETUP

The consolidated porous medium used in this experiment was a smooth finish, commercially available, fired-clay ceramic stone that was 1.5 cm thick, 42 cm long, and 40 cm wide. The stone was set at an inclination of 12.5 degrees with the horizontal. Using a calibrated syringe, a specified amount of water was introduced into one end of a flexible tube having an internal cross-sectional area of 0.2 cm². The other end of the tube was closed to retain the water in the tube. The water inside the tube was positioned near the end of the tube from which the water was to be introduced onto the porous surface. The tube was positioned onto the porous stone and water was released onto the porous plane. The distance that the water traveled on the porous plane before being completely imbibed was noted. This experiment was repeated four times at different regions on the porous plane using three different quantities of water (0.5, 0.7, and 0.9 cm³). In doing so the variations in the experimentally observed penetration length associated with variations in the mechanism to introduce water, or porous medium property variations can be quantified, and the systematic variation in the mean penetration length due to varying the quantity of water applied can be better judged. The thinning of the water film at its rear visible limit, and the advancement of the trailing edge of water as the front end slows was observed and was qualitatively similar to the numerical simulation shown in Figures 3-6(a) and (b), and 4-2(a) and (b). The mean and standard deviations of the experimentally observed penetration lengths are reported in Table 5-1.

5.2 ESTIMATION OF IMBIBITION COEFFICIENT

The porous surface used in the experiments was positioned horizontally, and a small quantity of water was applied. The time required for the water to be completely imbibed into the matrix was recorded. This time is related to the Green-Ampt imbibition coefficient [Eq. (3-16a,b)]

$$D_{GA} = \frac{\left(\frac{\text{Volume of Water}}{\text{Area of Application}} \right)^2}{4 \times \text{Time for Complete Imbibition}} \quad (5-1)$$

A cubic centimeter of water applied over a region 1.75 cm in diameter was fully imbibed in 15 s. This yields an estimate of the imbibition coefficient D_{GA} of 3.0×10^{-7} m²/s. The limited thickness of the porous specimen (1.5 cm) did not interfere with the measurement technique as the wetting front depth

Table 5-1. Experimentally observed penetration lengths

Volume of Water cm ³	Penetration Length	
	Mean cm	Standard Deviation cm
0.5	11.9	1.2
0.7	18.1	2.7
0.9	28.0	2.8

inferred from Eq. (3-16a) was much less than 1.5 cm. This estimate was observed repeatedly at different locations on the initially dry porous medium. Admittedly, with the assumption of 1D Green-Ampt imbibition, this is a rough estimate of the imbibition characteristics of the porous medium. However, in view of the lack of readily available techniques for directly measuring the hydraulic conductivity for consolidated porous medium, this is a useful characterization of imbibition characteristics of the porous medium. A direct inference of parameters governing porous medium behavior (albeit simplified) makes possible “uncalibrated” predictions using the simple model in Section 3.2.3. There is no adjustable parameter in the predictions of the penetration length made in the next section.

5.3 PREDICTIONS AND OBSERVATIONS OF PENETRATION LENGTH

The model based on a simplified Green-Ampt representation of the imbibition process (in Section 3.2.3) is used to predict the penetration length and to compare that length with the experimentally observed penetration length. The boundary conditions to simulate the experiment are a specified height of the water film at the upstream end of the porous medium for the amount of time it takes to apply a specified amount of water. Since the model is 2D, the side of a square of an area equal to that of the circular water application tubes internal area is the specified height of water [i.e., $(2.00 \times 10^{-5})^{1/2}$ m]. In the 2D model, when the total area of water applied to the porous medium becomes equal to the volume of water applied in the experiment, divided by $(2.00 \times 10^{-5})^{1/2}$ m, the boundary condition is switched to zero water height. At the downstream end, the height of the water is taken to be zero. The downstream zero boundary condition is passive insofar as the computational domain was always larger than the penetration length. With this boundary condition the evolution of the water body is simulated. The maximum distance to which the leading edge of water travels (the penetration length) is noted for the three different amounts of water applied. The model predictions of penetration length are shown by the diamond symbol in Figure 5-1. The mean of the experimentally observed penetration length and the experimentally observed one standard deviation envelope around the mean are shown by the circles with error bars in Figure 5-1. The correct order of magnitude of the penetration length is predicted by the model. This quantitative comparison of the experiment with the model indicates that interaction of the imbibition time scales and viscous water flow time scale in determining the distance to which water can travel outside the porous medium is well represented in the simple model. The limited size of the porous specimen limits the quantity of water that can be applied in the experiment.

12.5 degree incline

5-3

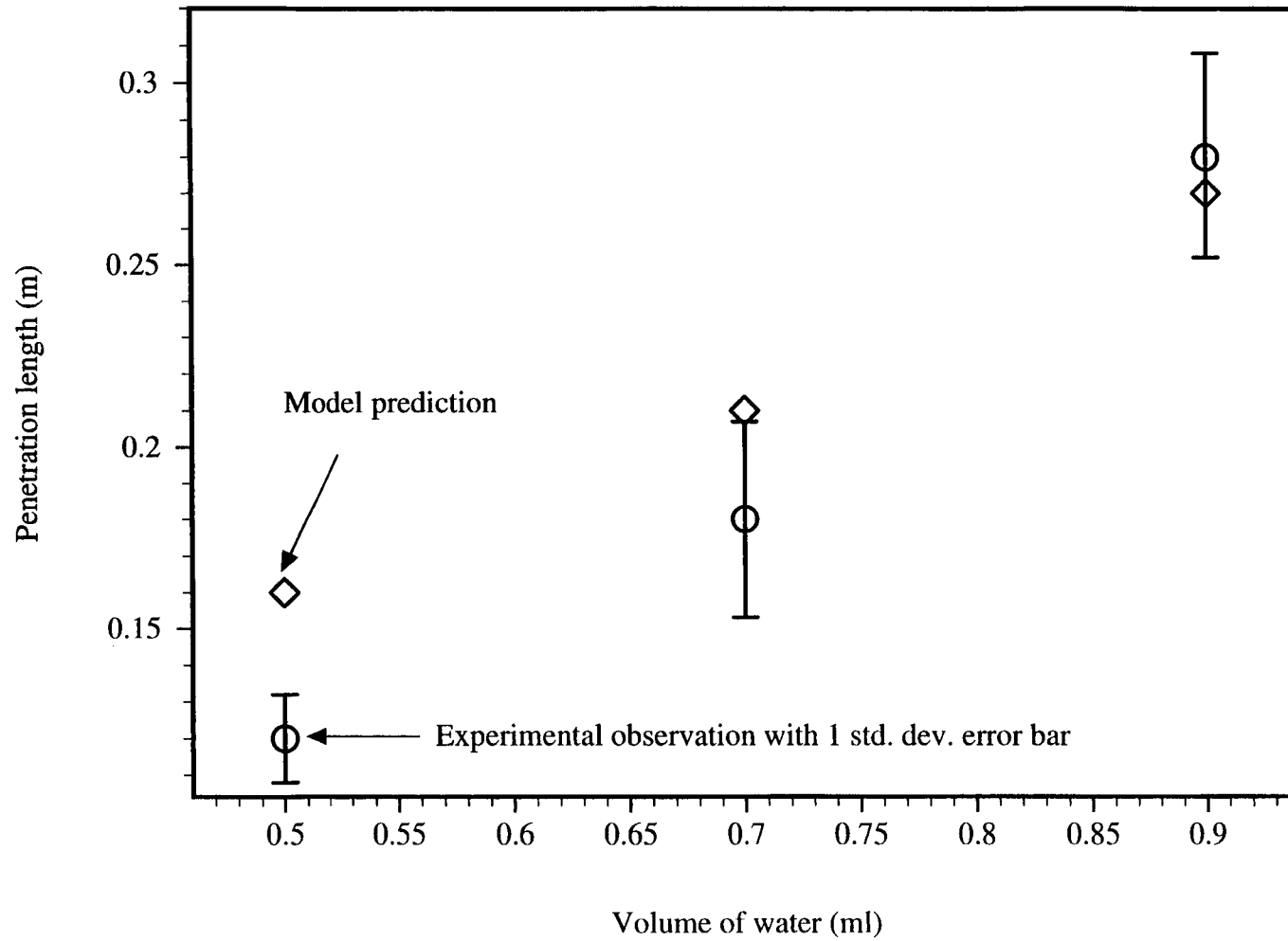


Figure 5-1. Penetration length as a function of volume of water applied—experimental observations and model predictions

Needless to say, these experiments only provide preliminary support of the simplified models ability to simulate water "dripping" on an unsaturated porous medium. Further experiments with different types of consolidated material and detailed measurements of unsaturated constitutive properties of consolidated porous materials are clearly needed.

6 DISCUSSION

That fractures in low permeability porous media above the water table in arid zones can be important conduits for the flow of water is readily observable in a tunnel beneath Rainier Mesa (Russel et al., 1987) in southern Nevada. The time-scales associated with the downward movement of water in consolidated porous media at YM are large because of the low hydraulic conductivities. Water movement through the consolidated porous matrix cannot explain the geochemical data at YM. Other studies have concluded that fracture induced flow is potentially the main mechanism of bringing water to the waste package in the proposed repository at YM, and transporting radionuclides dissolved in water to the water table (Buscheck et al., 1991; Nitao and Buscheck, 1992; Buscheck and Nitao, 1993). Motivated by these observations, water dripping down a fracture under gravity and imbibing into the porous matrix on account of capillary tension, was modeled in this report.

The fluid outside the porous matrix, dripping down a fracture, was modeled using the thin-film approximation that incorporates the effects of energy supplied to the fluid by gravity and energy dissipated due to viscosity. The imbibition of water was represented by three different methods. The first idealization was to simply represent it as a first order loss term. This was done to understand the behavior of the thin film equation with a sink term. The similarity solutions derived with this representation predicted the existence of a distinct penetration length, and also provided a way to verify numerical approximations. The second, and more realistic representation of imbibition, was made employing a Green-Ampt approximation for the moisture inside the porous matrix. This imbibition representation is simple to implement numerically, and the imbibition rate can be experimentally inferred relatively easily. The third, and most detailed representation of the imbibition process, was made by Richards' equation. The evolution of water outside the porous medium, and the moisture inside the porous medium, was simulated with the different imbibition representations. The analysis was performed in two spatial dimensions and temporal evolutions were studied.

The effects of surface tension at the moving interface between water, porous medium, and air, at both the front and the rear extremity of water outside the porous medium has not been analyzed here. Since the solution for the thin-film of water tends to have a sharp front at the leading edge [Figures 3-6(a) and 4-2(a)], the effect of surface tension may be much more pronounced there, and can be expected to counter the sharp front. The mathematical representation of the physical processes at such a moving contact with high curvature is being explored in the fluid mechanics literature for flow on impervious solids (e.g., Dussan, 1979; Goodwin and Homsy, 1991; Kalliadasis and Chang, 1994). The important effect of surface tension incorporated in this study is within the porous medium, which controls the imbibition into the low-permeability porous medium on which the thin-film of water is moving. The effects of gravity and viscosity on the water outside the porous medium were considered in detail. It was demonstrated that the existence of distinct penetration lengths beyond which water cannot travel outside the porous medium is not dependent on the effects of surface tension on the water body outside the porous medium. The effect of surface tension may alter the penetration length significantly if the dimensions of the water outside the porous medium are small enough. The Bond number ($\rho g l^2 /$ coefficient of surface tension of water) based on the transverse dimension of the film of water in the experiment ($l = 4.4721 \times 10^{-3}$ m) is about 50, which probably explains why the model predictions without surface tension effects are yielding the right magnitude of the penetration length (Figure 5-1). That the prediction is better for larger amounts of water applied may be due to the lessening of surface tension effects. The fact that the simple model of viscous-gravity flow coupled with Green-Ampt imbibition is able to predict the penetration length is not altogether surprising, considering that previous studies on impervious surfaces have reported good agreement with

observations (Smith, 1973; Huppert, 1982; Lister, 1992), and that the time scale of the imbibition process, the additional process incorporated here, is experimentally determined in this work.

The porous medium employed in the experiment reported in section 5 had a very smooth finish. Otherwise, surface roughness effects, that have not been considered in this analysis, may be very important. Mild undulations in the porous surface are easily dealt with by considering x_1 (Figure 2-1) to be aligned with the mildly undulating surface. The value of the angle α between a tangent at the surface and the horizontal direction may be considered to be varying with spatial coordinates, rendering the value c [Eq. (2-9a)] to be varying smoothly in space. A mild variation is one in which the time scale associated with a water element experiencing its effects is larger than the time scale associated with the viscous momentum diffusion time scale associated with the film thickness. Fine scale variations are ones in which the time scale associated with a water element experiencing its effects is smaller than the time scale associated with viscous momentum diffusion across the film thickness. Such variations may result in considerably greater viscous dissipation of energy which may be represented by an effective viscosity by multiplying the dynamic viscosity in Eq. (2-9a) by a "roughness coefficient," that needs to be empirically determined. Turbulent effects are parameterized by replacing ch^2 in Eq. (2-9a) by a general velocity representation, $c_1 h^{c_2}$, where c_1 and c_2 are to be empirically determined. Cundy and Tonto (1985) and Luce and Cundy (1992) discuss these parameterizations. In addition to these effects, it is to be expected that interfacial surface tension effects will play an important role in conjunction with surface roughness effects, which will create more curvature at the air-water interface. Rasmussen (1991) has analyzed surface tension effects at the air water interface, for steady-state flow on impervious surfaces. An analysis combining the unsteady imbibition-viscous-gravity effects with a moving air-water interface, as analyzed here, with dynamic air-water interfacial surface tension and air-water-solid contact line effects, on an irregular unsaturated porous surface, needs to be undertaken to provide a comprehensive understanding of the phenomenon of water dripping down fractures in consolidated porous medium.

The goal of this work is to understand flow in fractured consolidated porous medium with fractures large enough for viscous and gravity effects to be important for flow inside the fractures. A parallel plate model of fracture flow in an unsaturated porous medium would require considering imbibition on both surfaces as long as the flux is large enough to sustain a fully occupied fracture. The transition from a fully saturated fracture to a partially occupied fracture would have to be determined. A parallel plate fracture at an angle with the vertical, subjected to incipient ponding conditions would behave like the flow with a Dirichlet upstream boundary condition, analyzed in Section 3.1.1 (Figure 3-4). The distance that the water supplied during a rainfall event can travel in an open exposed void may be important to know in assessing the environmental consequences of waste disposal in fractured unsaturated porous medium. Equations (3-5), (3-7), (3-11), and (3-12) provide a simple estimate of that, assuming a linear representation of imbibition into the porous matrix. For a Green-Ampt description of the imbibition process, a simple numerical model is presented in Section 3.2.3, and compared to experimental observations in Section 5. If the penetration length is much smaller than the depth at which a waste disposal scheme lies in fractured porous medium, then the impact of such flows may not be very important. After the water gets into the matrix, it is no longer in the fast downward pathway (assuming the porous medium to be of small permeability), and will experience other influences like thermal effects and evaporation. The penetration length may be greater than the depth of the waste disposal scheme; however, the time required for water to get there may be so large, that the influence is again not very important. On the other hand, if the penetration length is rapidly attained and is greater than the waste disposal depth, the influence of such waters will be potentially important in transporting contaminants.

While the previous discussion pertains to water entering the vadose zone from the surface, the effect of fractures on the redistribution of water inside the vadose zone is also of concern. For example, a fracture connected to a perched water zone has the potential to drain it. The water from the perched zone, traveling down the fracture, will reenter the unsaturated porous matrix surrounding the fracture. This nonequilibrium process of formation of perched water zones and their drainage by fractures can be simulated using the model developed here. In considering the nonisothermal effects of the emplacement of radioactive waste in a repository, the effect of evaporation of water in delaying the corrosion of waste canisters is an important parameter in assessing the repository performance. Of concern is the dripping of condensed water down fractures in the porous matrix around the waste package (Buscheck and Nitao, 1993), which may be assessed using the presented model.

6.1 FRACTURE EFFICACY NUMBER

Consider the flow in a fractured porous medium with a fracture oriented at an angle α to the horizontal, with an aperture r and length L (with a unit transverse dimension). For the Green-Ampt imbibition model in Eq. (3-16), the time scale t_I associated with imbibition of the water in the fracture by the porous matrix is given by

$$t_I = \frac{r^2}{4D_{GA}} \quad (6-1a)$$

The imbibition coefficient D_{GA} defined in Eq. (3-16b), is linearly related to the squared sorptivity of a porous medium [$4D_{GA} = (\text{Sorptivity})^2$] as discussed in Phillip (1969). Zimmerman and Bodvarsson (1992) present expressions relating the sorptivity to commonly used parameters of hydraulic conductivity-suction head-moisture content functions. The substitution of sorptivity in the model with Green-Ampt imbibition extends it to general hydraulic conductivity models, under the assumption that gravity plays an unimportant role in the transport of moisture inside the porous matrix, compared to its action on water in fractures. From the thin-film approximation [Eqs. (2-9a,b)], it follows that the time scale of water movement inside the fracture under the influence of gravity and viscosity, t_A is given by

$$t_A = \frac{\mu L}{\rho g \sin(\alpha) r^2} \quad (6-1b)$$

The ratio of these two time scales may be called the "fracture efficacy number"

$$F_e(r, L) \equiv \frac{t_I}{t_A} \quad (6-1c)$$

The faster the process of imbibition of water into the porous medium, as compared to the advection of water along the length of a fracture, the smaller the likelihood of water traveling the length of the fracture, the smaller is the "fracture efficacy number" in Eq. (6-1c). Substituting for the distinct time scales [Eqs. (6-1a,b)] into Eq. (6-1c)

$$F_e = \frac{\rho g \sin(\alpha) r^4}{(\text{Sorptivity})^2 \mu L} \tag{6-1d}$$

$$= \frac{\rho g \sin(\alpha) r^4}{4 D_{GA} \mu L} = \frac{\rho g \sin(\alpha) r^4}{2 K_{GA} (\theta_w - \theta_b) \Psi_f \mu L}$$

A fracture efficacy number of much larger than one implies that water can travel over the length of the fracture without getting imbibed into the porous matrix. If water finds its way into a fracture with F_e much larger than one, the fracture will serve as a conduit transporting the water over its entire length. In modeling flow in highly fractured porous medium, priority should be given to modeling the fluid flow in persistent fractures with large fracture efficacy numbers.

7 SUMMARY AND RECOMMENDATIONS

The objective of this study was to model water dripping down an unfilled fracture in an unsaturated porous medium. This was accomplished by describing flow in the fracture by the thin film approximation and coupling it to the porous medium by a loss term. The results of this study are summarized below:

- Similarity solutions for the spatial-temporal evolution of fluid flowing down an unsaturated porous incline were found with a linear representation of the imbibition process (Section 3.1 and Figure 3-1).
- The maximum distance a finite amount of water can travel down a porous incline before being completely imbibed into it (the penetration length) was expressed by simple analytical relationships that show how the penetration length increases with an increase in the amount of water applied, angle of inclination, and density of water, and how it decreases with an increase in the dynamic viscosity of water and the rate of imbibition into the matrix (Section 3.1).
- Numerical approximations for modeling the flow of thin-films of water were verified by comparing with similarity solutions, including the effects of an idealized linear imbibition rate, and without any imbibition (Sections 3.2.1 and 3.2.2).
- By employing a Green-Ampt representation for imbibition of water into the unsaturated porous medium, the spatial-temporal evolution of water was simulated. The longitudinal extent of the film initially expands as the water body moves down the unsaturated porous medium. The rear limit of the film then advances, causing a decrease in the longitudinal dimension of the film, and meets the leading edge of the film when it is completely imbibed into the porous matrix (Section 3.2.3).
- The imbibition coefficient governing Green-Ampt model-based evaluation of imbibition of water into the unsaturated porous matrix was experimentally estimated, and model predictions of the penetration length made. That the model successfully captures the dynamics of the viscous-gravity-imbibition fluid flow process is reflected in its ability to predict the experimentally observed penetration lengths (Sections 5.2 and 5.3, and Figure 5-1).
- The fracture efficacy number was defined as the time scale over which water in a fracture becomes imbibed into the porous matrix divided by the time scale over which the water travels the fracture length. Simple analytical expressions for these time scales yield an expression for the fracture efficacy number. Fractures with fracture efficacy numbers greater than one are potentially important conduits for water flow over their length. (Section 6.1).

Specific recommendations for future work are:

- Evaluate the potential for water dripping down fractures in distinct geologic units at YM by determining fracture efficacy numbers, using realistic data for fracture apertures, lengths, orientations, and matrix sorptivity.

- Examine the influence of fracture surface roughness in conjunction with dynamic air-water interfacial tension and air-water-solid contact line effects
- Perform experiments with well-characterized porous medium to critically judge our ability to estimate rates of water movement in unfilled fractures in unsaturated porous medium
- Compare water movement rates resulting from the approach developed in this work with the more popular models based on the equivalent continuum, dual continuum, and dual permeability approaches (described in Section 1.3) to evaluate their applicability in modeling water dripping down an unfilled fracture
- Interpret field geochemical data discussed in Section 1.2 with distinct modeling approaches to evaluate their applicability in determining regulatory performance measures to assess the feasibility of the HLW repository at YM

8 REFERENCES

- Ababou, R. 1991. *Approaches to Large Scale Unsaturated Flow in Heterogeneous, Stratified, and Fractured Geologic Media*. NUREG/CR-5743. Washington, DC: Nuclear Regulatory Commission.
- Ababou, R., and L.W. Gelhar. 1988. A high-resolution finite difference simulator for 3D unsaturated flow in heterogeneous media. *Computational Methods in Water Resources*. Elsevier and Computational Mechanics Publications 1: 173-178.
- Acheson, D.J. 1989. *Elementary Fluid Dynamics*. Oxford, United Kingdom: Clarendon Press.
- Anderson, J., and A.M. Shapiro. 1983. Stochastic analysis of one-dimensional steady state unsaturated flow: A comparison of Monte Carlo and perturbation methods. *Water Resources Research* 19(1): 121-133.
- Baca, R.G., and S.O. Magnuson. 1992. *FLASH—A Finite Element Computer Code for Variably Saturated Flow*. EGG-GEO-10274. Idaho Falls, ID: Idaho National Engineering Laboratory: EG&G Idaho, Inc.
- Baca, R.G., I.P. King, and W.R. Norton. 1978. Finite element models for simultaneous head and moisture transport in unsaturated soils. *Proceedings of the Second International Conference on Finite Elements in Water Resources*. London, UK: Pentech Press: Imperial College.
- Baca, R.G., R.C. Arnett, and D.W. Langford. 1984. Modeling fluid flow in fractured-porous masses by finite element techniques. *International Journal for Numerical Methods in Fluids* 4: 337-348.
- Bear, J. 1972. *Dynamics of Fluids in Porous Media*. New York: Dover.
- Beavers, G.S., and D.D. Joseph. 1967. Boundary condition at a naturally permeable wall. *Journal of Fluid Mechanics* 30, 197-207.
- Beavers, G.S., E.M. Sparrow, and R.A. Magnuson. 1970. Experiments on coupled parallel flows in a channel and a bounding medium. *ASME Journal of Basic Engineering* 92: 843-848.
- Beavers, G.S., E.M. Sparrow, and B.A. Masha. 1974. Boundary conditions at a porous surface which bounds a fluid flow. *AIChE Journal* 20: 596-597.
- Beven, K., and P. Germann. 1981. Water flow in soil macropores, 2; A combined flow model. *Journal of Soil Science* 32: 15-29.
- Beven, K., and P. Germann. 1982. Macropores and water flow in soils. *Water Resources Research* 18(5): 1,311-1,325.
- Brown, D.M., and L.W. Gelhar. 1985. *The Hydrology of Fractured Rocks: A Literature Review*. Ralph M. Parsons Laboratory Report No. 304. Cambridge, MA: Massachusetts Institute of Technology.

- Burgers, J.M. 1974. *The Nonlinear Diffusion Equation*. Boston, MA: Reidel.
- Buscheck, T.A., and J.J. Nitao. 1993. The analysis of repository-heat-driven hydrothermal flow at Yucca Mountain. *Proceedings of the 4th High-Level Radioactive Waste Management Conference*. New York, NY: American Society of Civil Engineers.
- Buscheck, D.A., J.N. Nitao, and D.A. Chestnut. 1991. The impact of episodic nonequilibrium fracture-matrix flow on geological repository performance. *Proceedings on Nuclear Waste Packaging, FOCUS '91*. LaGrange Park, IL: American Nuclear Society.
- Celia, M.A., E.T. Bouloutas, and R.L. Zarba. 1990. A general mass-conservative solution for the unsaturated flow equation. *Water Resources Research* 26(7): 1,483-1,496.
- Chen, C.L. 1970. Surface irrigation using kinematic wave method. No. IR1. *Journal of the Irrigation and Drainage Division of American Society of Civil Engineers* 96: 39-46.
- Chuang, Y., W.R. Haldeman, T.C. Rasmussen, and D.D. Evans, 1990. *Laboratory Analysis of Fluid Flow and Solute Transport Through a Variably Saturated Fracture Embedded in Porous Tuff*. NUREG/CR 5482. Washington, DC: Nuclear Regulatory Commission.
- Clothier, B.E., and I. White. 1981. Measurement of sorptivity and soil-water diffusivity in the field. *Soil Science Society American Journal* 45: 241-245.
- Clothier, B.E., J. Knight, and I. White. 1981. Burgers equation: Application to field constant flux infiltration. *Soil Science* 132: 255-261.
- Cooley, R.L. 1983. Some new procedures for numerical solution of variably saturated flow problems. *Water Resources Research* 19(5): 1,271-1,285.
- Cundy, T.W., and S.W. Tonto. 1985. Solution to the kinematic wave approach to overland flow routing with rainfall excess given by Philip's equation. *Water Resources Research* 21(8): 1,132-1,140.
- Davidson, M.R. 1994. A Green-Ampt model of infiltration in a cracked soil. *Water Resources Research* 20(11): 1,685-1,690.
- Dussan, V. 1979. On the spreading of liquids on solid surfaces: Static and dynamic contact lines. *Annual Review of Fluid Mechanics* 11: 371-400.
- Finlayson, B.A. 1985. *Nonlinear Analysis in Chemical Engineering*. New York, NY: McGraw-Hill International Book Company.
- Freeze, R.A. 1991. Hydrogeologic issues at Yucca Mountain: Findings of a DOE peer review team. *Proceedings of Workshop V: Flow and Transport Through Unsaturated Fractured Rock—Related to High-Level Radioactive Waste Disposal*. NUREG/CP-0040. Washington, DC: Nuclear Regulatory Commission.

- Gardner, W.R. 1958. Some steady state solutions of the unsaturated moisture flow equation with application to evaporation from a water table. *Soil Science* 85(4): 228-232.
- Gelhar, L.W. 1993. *Stochastic Subsurface Hydrology*. Englewood Cliffs, NJ: Prentice-Hall.
- Germann, P., and K. Beven. 1981a. Water flow in soil macropores, 1, An experimental approach. *Journal of Soil Science* 32: 1-13.
- Germann, P., and K. Beven. 1981b. Water flow in soil macropores, 3, A statistical approach. *Journal of Soil Science* 32: 31-39.
- Ghosh, A., S.-M. Hsiung, G.I. Ofoegbu, and A.H. Chowdhury. 1994. *Evaluation of Computer Codes for Compliance Determination Phase II*. CNWRA 94-001. San Antonio, TX: Center for Nuclear Waste Regulatory Analyses.
- Goodwin, R., and G.M. Homsy. 1991. Viscous flows down a slope in the vicinity of a contact line. *Physics of Fluids* A3: 515-528.
- Green, W.H., and G.A. Ampt. 1911. Studies in soil physics, I, Flow of air and water through soils. *Journal of Agricultural Science* 4: 1-24.
- Gureghian, A.B., D.S. Ward, and R.W. Cleary. 1979. Simultaneous transport of water and reacting solutes through multilayered soils under transient unsaturated flow conditions. *Journal of Hydrology* 41: 253-278.
- Henderson, F.M., and R.A. Wooding. 1964. Overland flow and groundwater flow from a steady rainfall of finite duration. *Journal of Geophysical Research* 69: 1,531-1,540.
- Hunt, B. 1983. *Mathematical Analysis of Groundwater Resources*. Boston, MA: Butterworth.
- Huppert, H.E. 1982. Flow and instability of a viscous current down a slope. *Nature* 300: 427-429.
- Huyakorn, P.S., and G.F. Pinder. 1983. *Computational Methods in Subsurface Flow*. New York, NY: Academic Press.
- Kalliadasis, S., and H.C. Chang. 1994. Apparent dynamic contact angle of an advancing gas-liquid meniscus. *Physics of Fluids* 6(1): 12-23.
- Klavetter, E.A., and R.R. Peters. 1988. A continuum model for water movement in an unsaturated fractured rock mass. *Water Resources Research* 24: 416-430.
- Li, R.M., D.B. Simmons, and M.A. Stevens. 1975. Nonlinear kinematic wave approximation for water routing. *Water Resources Research* 11(2): 245-252.
- Lister, J.R. 1992. Viscous flow down an inclined plane from point and line sources. *Journal of Fluid Mechanics* 242: 631-653.

- Luce, C.H., and T.W. Cundy. 1992. Modification of the kinematic wave-Philip infiltration overland flow model. *Water Resources Research* 28(4): 1,179-1,186.
- MacCormack, R.W. 1969. *The Effect of Viscosity in Hypervelocity Impact Cratering*. AIAA Paper No. 69-354.
- Manteufel, R.D., M.P. Ahola, D.R. Turner, and A.H. Chowdhury. 1993. *A Literature Review of Coupled Thermal-Hydrologic-Mechanical-Chemical Processes Pertinent to the Proposed High-Level Nuclear Waste Repository at Yucca Mountain*. NUREG/CR-6021, CNWRA 92-011. Washington, DC: Nuclear Regulatory Commission.
- Mantoglou, A., and L.W. Gelhar. 1987. Capillary tension head variance, mean soil moisture content, and effective specific soil moisture capacity of transient unsaturated flow in stratified soils. *Water Resources Research* 23(1): 47-56.
- Martys, N., D.P. Bentz, and E.J. Garloczi. 1994. Computer simulation of the effective viscosity in Brinkman's equation. *Physics of Fluids* 6(4): 1,434-1,439.
- Montazer, P., and W.E. Wilson, 1984. *Conceptual Hydrologic Model of Flow in the Unsaturated Zone, Yucca Mountain, Nevada*. U.S. Geological Survey. U.S. Geological Survey Water Resources Investigations Report No. 84-4345.
- Mualem, Y. 1984. Anisotropy of unsaturated soils. *Soil Science Society of America Journal* 48: 505-509.
- Neuman, S.P. 1973. Saturated-unsaturated seepage by finite elements. *Journal of the Hydraulics Division* 11(12): 2,233-2,250.
- Nitao, J.N., and T.A. Buscheck. 1991. Infiltration of a liquid front in an unsaturated porous medium. *Water Resources Research* 27: 2,099-2,112.
- Nitao, J.N., T.A. Buscheck, and D.A. Chestnut. 1992. The implications of episodic nonequilibrium fracture-matrix flow on site suitability and total system performance. *Proceedings of the Third International High Level Radioactive Waste Management Conference*. LaGrange Park, IL: American Nuclear Society: 279-296.
- Nuclear Regulatory Commission. 1983. *Federal Register*. Washington, DC: U.S. Government Printing Office. 48(120).
- Nuclear Regulatory Commission. 1991. Disposal of high-level radioactive wastes in geologic repositories. *Code of Federal Regulations, Title 10, Part 60*. Washington, DC: U.S. Government Printing Office.
- Norris, A.E. 1989. The use of chlorine isotope measurement to trace water movement at Yucca Mountain. *Proceedings of Topical Meeting on Nuclear Waste Isolation in the Unsaturated Zone, Las Vegas, NV, September 17-21, 1989*. LaGrange Park, IL: American Nuclear Society.

- Paniconi, C., and E.F. Wood. 1993. A detailed model for simulation of catchment scale subsurface hydrologic processes. *Water Resources Research* 29(6): 1,601-1,620.
- Peters, R.R., E.A. Klavetter, I.J. Hall, S.C. Blair, G.W. Heller, and G.W. Gee. 1984. *Fracture and Matrix Characteristics of Tuffaceous Materials from Yucca Mountain, Nye County, Nevada*. SAND84-1471. Albuquerque, NM: Sandia National Laboratories.
- Peters, R.R., J.H. Gauthier, and A.L. Dudley. 1986. *The Effect of Percolation Rate on Water Travel Time in Deep, Partially Saturated Zones*. SAND85-0854C. Albuquerque, NM: Sandia National Laboratories.
- Peyret, R., and T.D. Taylor. 1983. *Computational Methods for Fluid Flow*. New York, NY: Springer-Verlag.
- Philip, J.R. 1969. Theory of infiltration. *Advances in Hydrosience*. V.T. Chow, ed. New York, NY: Academic Press.
- Philip, J.R. 1974. Recent progress in the solution of nonlinear diffusion equations. *Soil Science* 117: 257-264.
- Polmann, D.J., E.G. Vomvoris, D. Mclaughlin, E.M. Hammick, and L.W. Gelhar. 1988. *Application of Stochastic Methods to the Simulation of Large-Scale Unsaturated Flow and Transport*. NUREG/CR-5094. Washington, DC: Nuclear Regulatory Commission.
- Quade, J., and T.E. Cerling. 1990. Stable isotopic evidence for a pedogenic origin of carbonates in trench 14 near Yucca Mountain, Nevada. *Science* 250: 1,549.
- Rasmussen, T.C. 1991. Steady flow and travel times in partially saturated fractures using a discrete air-water interface. *Water Resources Research* 27(1): 67-76.
- Richards, L.A. 1931. Capillary conduction of liquids through porous medium. *Physics* 1: 318-333.
- Rogers, C., and W.F. Ames. 1989. *Nonlinear Boundary Value Problems in Science and Engineering*. New York, NY: Academic Press.
- Russel, C.E., J.W. Hess, and S.W. Tyler. 1987. Hydrogeologic investigations of flow in fractured tuffs, Rainier Mesa, Nevada Test Site. *Flow and Transport Through Unsaturated Fractured Rock*. D.D. Evans and T.J. Nicholson, eds. Washington, DC: American Geophysical Union: 43-50.
- Saffman, P. 1971. On the boundary condition at the surface of a porous medium. *Studies in Applied Mathematics* 50: 93-101.
- Schumacher, W. 1864. *Die Physik des Bodens*. Berlin, Germany.

- Scott, R.B., R.W. Spengler, S. Diehl, A.R. Lappin, and M.P. Chornack. 1983. Geologic character of tuffs in the unsaturated zone at Yucca Mountain, southern Nevada. *Role of the Unsaturated Zone in Radioactive and Hazardous Waste Disposal*. J.W. Mercer, P.S.C. Rao, and I.W. Marine, eds. Ann Arbor, MI: Ann Arbor Science Publishers: 289-335.
- Smith, P.C. 1973. A similarity solution for slow viscous flow down an inclined plane. *Journal of Fluid Mechanics* 58: 275-288.
- Smith, R.E., and R.H.B. Hebbert. 1979. A Monte Carlo analysis of hydrologic effects of spatial variability of infiltration. *Water Resources Research* 15(2): 419-429.
- Smith, R.E., and D.A. Woolhiser. 1971. Overland flow on an infiltrating surface. *Water Resources Research* 7(4): 899-913.
- Szabo, B.J., and T.K. Kyser. 1990. Ages and stable isotope compositions of secondary calcite and opal in drill cores from tertiary volcanic rocks of the Yucca Mountain area, Nevada. *Geological Society of America Bulletin* 102: 1,714-1,719.
- Taylor, A.B. 1986. *Mathematical Models in Applied Mechanics*. Oxford, United Kingdom: Clarendon Press.
- Taylor, G.I. 1971. A model for the boundary condition of a porous material, Part 1. *Journal of Fluid Mechanics* 49: 319-326.
- Therrien, R. 1992. *Three-Dimensional Analysis of Variably Saturated Flow and Solute Transport in Discretely Fractured Porous Media*. Ph.D. Thesis. Ontario, Canada: University of Waterloo.
- Travis, B.J., S.W. Hodson, H.E. Nuttall, T.L. Cook, and R.S. Rundberg. 1984. *Preliminary Estimates of Water Flow and Radionuclide Transport in Yucca Mountain*. LA-UR-84-40. Los Alamos, NM: Los Alamos National Laboratory.
- Updegraff, C.D., C.E. Lee, and D.P. Gallegos. 1991. *DCM3D: A Dual-Continuum, Three-Dimensional, Ground-Water Flow Code for Unsaturated, Fractured, Porous Media*. NUREG/CR-5536. Washington, DC: Nuclear Regulatory Commission.
- U.S. Department of Energy. 1988. *United States Site Characterization Plan, Yucca Mountain Site, Nevada Research and Development Area, Nevada*. DOE/RW-0199. Washington, DC: U.S. Department of Energy.
- U.S. Environmental Protection Agency. 1991. Environmental radiation protection standards for management and disposal of spent nuclear fuel, high-level and transuranic radioactive wastes. *Code of Federal Regulations, Title 40, Part 191*. Washington, DC: U.S. Government Printing Office.
- van Genuchten, M.T., and D.R. Nielsen. 1985. On describing and predicting the hydraulic properties of unsaturated soils. *Annual Geophysics* 3(5): 615-628.

- Waddell, R.K., J.H. Robison, and R.K. Blankennagel. 1984. *Hydrology of Yucca Mountain and Vicinity, Nevada-California: Investigative Results Through Mid-1983*. Water Resources Investigative Report 84-4267. U.S. Geological Society.
- Wang, J.S., and T.N. Narasimhan. 1985. Hydrologic mechanisms governing fluid flow in a partially saturated porous medium. *Water Resources Research* 21: 1,861-1,874.
- Water, Waste, and Land, Inc., 1986. *Analysis of Observed Flow Between Test Wells USW G-1 and USW UZ-1*. Mini Report No. 6. Water, Waste, and Land, Inc.
- Whitham, G.B. 1974. *Linear and Nonlinear Waves* New York, NY: John Wiley and Sons.
- Wittmeyer, G., S. Mohanty, R. Codell, and T. McCartin. 1993. *Yucca Mountain Test Case: Predicted Water Content Profiles for Borehole USW UZ16*. Stockholm, Sweden: INTRAVAL Workshop.
- Yang, I.C. 1992. Flow and transport through unsaturated rock—data from two test holes, Yucca Mountain, Nevada. *Proceedings of the Third International High Level Radioactive Waste Management Conference*. LaGrange Park, IL: American Nuclear Society: 732-737.
- Yeh, T.C. 1989. One dimensional steady state infiltration in heterogeneous soils. *Water Resources Research* 25(10): 2,149-2,158.
- Yeh, T.C., and D.J. Harvey. 1990. Effective hydraulic conductivity of layered sands. *Water Resources Research* 26(6): 1,271-1,279.
- Yeh, T.C., L.W. Gelhar, and A.L. Gutjahr. 1985. Stochastic analysis of unsaturated flow in heterogeneous soils, 1, Statistically isotropic media. *Water Resources Research* 21(4): 447-456.
- Zimmerman, R.W., and G.S. Bodvarsson. 1992. Semi-analytical treatment of fracture/matrix flow in a dual porosity simulator for unsaturated fractured rock masses. *Proceedings of the Third International High Level Radioactive Waste Management Conference*. LaGrange Park, IL: American Nuclear Society: 272-278.